University of Pécs
Doctoral School of Chemistry

Fundamentals of retention and mass flow in supercritical fluid chromatography

PhD thesis

Csanád Rédei

Supervisor:

Dr. Attila Felinger
professor of chemistry

Pécs, 2023

Contents

1

Introduction

Over the last few years, supercritical fluid chromatography (SFC) has gathered increased attention in a wide range of fields, including several academic and industrial areas. The technique has been employed extensively in analytical [1] and preparative chromatography [2–5], forensics [6], chiral separations and pharmaceutical applications [7] as well as the food industry [8]. Fundamental research is a smaller, but just as important part of the SFC community focusing on topics such as the effects of the mobile phase density or sample solvent and organic modifier adsorption [9–12]. The growing reputation of SFC can be associated with the rapid technological advancements of the last decade that made it a highly viable and comparable, but in the end a complementary technique besides liquid chromatography (LC).

SFC is usually characterized by having three major benefits over LC that can be derived from the physico-chemical properties of carbon dioxide: (1) it is more cost-effective and greener compared to LC due to lower organic solvent consumption; (2) the low viscosity of the mobile phase enables higher flow rates and thus shorter separations while also allowing rapid diffusion processes, reduced band broadening effects hence increased efficiency and (3) eluent strength is considered to be "well-tunable" by adjusting temperature, pressure and the concentration of the organic modifier in the mobile phase. However, it is important to note that depending on the experimental conditions, some of the advantageous properties may not be achieved at the same time, rather a compromise has to be made [13].

In SFC, the mobile phase is primarily composed of carbon dioxide besides the organic modifier and other additives. The solvents most often employed in LC are generally considered incompressible from a practical point of view. However, this is not the case for SFC due to the compressibility of carbon dioxide which results in

the variation of a series of thermodynamic and chromatographic properties along the system, e.g. mobile phase density, viscosity, temperature, velocity, solvation strength, retention factors and column efficiencies [2]. This introduces several difficulties to the work of SFC practitioners, which requires a deeper understanding and careful approach to resolve these effects, especially if no organic modifier is present in the mobile phase.

It is also understood that in SFC, the set and true volumetric flow rates differ from each other, that can become an important issue when trying to translate retention times and hold-up times into retention volumes and hold-up volumes, respectively. There are two requirements to do this conversion. One is the mass flow rate, that is the only flow parameter considered to remain constant throughout an SFC system [14]. Therefore, it can be utilized very well to determine actual volumetric flow rates by accurate, but careful measurements. The other would be the accurate knowledge of the hold-up time, another often overlooked parameter, whose determination has always been problematic in SFC, since the methods available are not as universal as in liquid chromatography.

2

Research objectives

The aim of the dissertation is to delve into the fundamentals of SFC, more specifically topics related to uncommon retention behavior observed in the case of neat carbon dioxide mobile phases, then the challenges of accurate mass flow rate measurements and lastly, exploring the options and limitations of hold-up time measurements. Our research objectives are described in detail as follows:

1. Studying the uncommon retention behavior of n-alkylbenzene homologues and the effect of different sample solvents on chromatographic efficiency:
    a) screening of different stationary phases and sample solvents (acetonitrile, heptane and methanol) to find anomalous retention behavior;
    b) determination of the single-component adsorption isotherms using the bi-Langmuir model and the inverse method (IM);
    c) determination of the competitive bi-Langmuir adsorption isotherms to understand the competition of the sample solvents and solutes;
    d) construction of a numerical model in order to simulate the competitive adsorption in the case of the real and two hypothetical compounds.
2. Scouting the effects of placement, experimental conditions and injections on mass flow measurements:
    a) studying the effect of placing the Coriolis flow meter (CFM) and pressure gauge at different positions in the SFC system;
    b) studying the effect of pressure and temperature on mass flow rate;
    c) studying the effect of injections on the mass flow rate at equilibrium.

3. Exploring the limitations of hold-up time measurements including the study of nitrous oxide as a new unretained marker:

    a) comparison of different compounds previously used as unretained markers in SFC;

    b) studying the effect of the amount of organic modifier in the mobile phase;

    c) surveying whether the stationary phase has any effect on the detection of hold-up time markers.

3

Literature review

3.1 The evolution of SFC

3.1.1 The first pioneers

The first rendition of supercritical fluid chromatography was reported in 1962, when Klesper et al. successfully separated a thermally unstable mixture of porphyrin derivatives using high-pressure gas chromatography (HPGC). The sample decomposed when they tried conventional gas chromatography (GC), but by using difluorodichloromethane and difluorochloromethane gases as mobile phases at high pressure, the separation was successful, and the sample was recovered at the end of the experiment [15].

A few years later, Sie et al. published several studies about the use of supercritical carbon dioxide as a mobile phase in HPGC systems, and discussed fluid-solid and fluid-liquid separation techniques in detail. They also contributed to the evolution of instrumentation by developing a pneumatic injector capable of injecting the sample under high-pressure and high-temperature conditions [16].

3.1.2 The development of SFC instruments

New developments of more sophisticated instrumentation were introduced towards the end of the 1960s, when the research group of Klesper reported a new system that could be considered a prototype of modern SFC, equipped with a back pressure regulator (BPR) that allowed for the system pressure to be controlled independently of the flow rate. In addition, the detector employed a high-pressure flow cell [17].

The work of Giddings et al. on dense gas chromatography (DGC) published in 1969 is of great importance. They reported GC separations performed at ultrahigh

pressures and laid the groundwork of unified chromatography (realized later in the 1980s), a concept to unite LC, GC and SFC separations in order to blur the boundaries between all three modes of chromatography. They proposed that since the density of the carrier gas at extremely high pressures is comparable to the density of liquids, the strong intermolecular interactions that are formed allow for non-volatile substances to turn volatile. This way they can be transferred to the gas phase and thus separated [16].

In 1970, Jentoft and Gouw developed an SFC system capable of pressure programming to study the separation of styrene oligomers and polycyclic aromatic hydrocarbons. In SFC, increasing the pressure results in an increase in the density of the mobile phase and consequently in the solubility of the sample components. Therefore, the programmable pressure can be compared to the gradient elution method of liquid chromatography [16, 18]. In 1972, a high-pressure fraction collection unit was developed, paving the way for the future of preparative SFC [19]. This line was taken further by Klesper and Hartman in 1977, who used a more sophisticated preparative SFC system to study the separation and fractionation of styrene oligomers and then identified the fractions by mass spectrometry (MS) [20, 21]. Consequently, the split between analytical and preparative SFC can be dated to the 1970s to later form their own branches.

3.1.3 Adapting different column technologies to SFC

In the following decade, chromatographers shifted their focus to studying the application and properties of different column technologies, besides instrumentation, that later contributed to the commercialization of SFC instruments [2]. Open tubular capillary columns, typically employed in GC, were introduced to SFC by Novotny et al. in 1981 [22]. These were fused silica capillary tubes with an inner diameter of 50 μm, where the inner wall was coated with a polymer that served as the stationary phase. They suggested that packed columns could not give high enough efficiencies due to the pressure gradient along the column that occurs as a result of the column packing and pressure drop. They theorized that a

smaller pressure drop along an open tubular capillary column would provide higher efficiencies as well as superior migration velocities for less volatile compounds compared to GC, while also maintaining a stronger "extraction effect" comparable to the solvation strength of LC. In terms of instrumentation, capillary SFC was more similar to GC, equipped with a syringe pump, a split injection valve, a column oven and a fixed restrictor, followed by a flame ionization detector (FID).

Unfortunately, technical limitations prevented the advancement of the technique. In modern SFC, pressure, temperature and organic modifier content can be controlled and adjusted independently of the flow rate or without suffering any negative consequences of operation. In capillary SFC, however, pressure was tied to the mobile phase velocity and due to the FID detector, the use of organic modifier resulted in a high background noise which hindered detection. Despite the efforts to overcome these obstacles, capillary SFC could not attract enough chromatographers to extend its application areas and so the technique was soon abandoned [16].

Packed column SFC was developed alongside capillary SFC and unlike the latter, it resembled the design and instrumentation of LC more. In 1982, Gere et al. successfully converted an LC system to operate as an SFC instrument [23]. They modified the pumping system to allow efficient operation with liquid carbon dioxide, installed a high-pressure detector cell and added a back pressure regulator downstream the detector. In the end, the entire system could operate in conditions up to 425 bar and 100 °C. All changes were reversible so the instrument could be returned to operate in LC mode again. Using the modified instrument, they demonstrated that SFC could produce reduced plate heights between 2.0 and 3.0 with polycyclic aromatic hydrocarbon (PAH) probe compounds and reversed phase stationary phases with 3, 5 and 10 μm particle sizes. Packed column SFC was sidelined for a while due to the strong marketing strategy promoting open tubular capillary SFC, but later regained popularity by the 1990s due to the versatile application possibilities of packed columns and continues to be the prevailing path of modern SFC to this day [16].

3.2 Characteristics of the supercritical state

When the pressure and temperature of a fluid exceed the critical pressure and temperature for that substance, then the substance is in a supercritical state. The phenomenon was first described by Charles Cagniard de la Tour in 1822 [2]. For pure substances, the easiest way to characterize phase transitions is by the means of phase diagrams, more specifically the vapor-liquid equilibrium curves in our case, that provide information about what happens in the vicinity of the critical point.

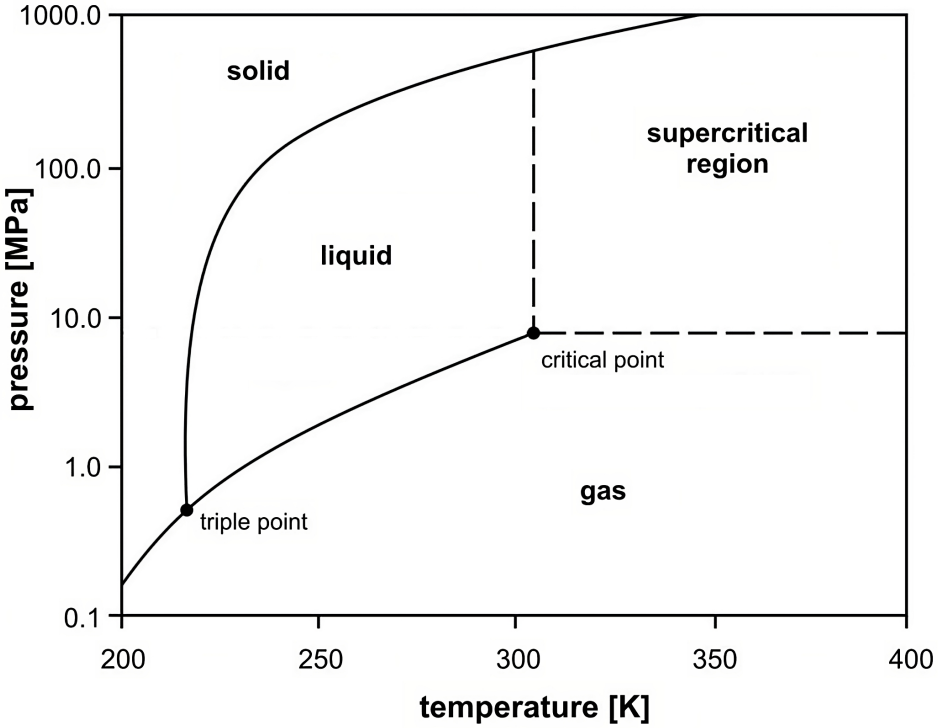

Fig. 3.1: The phase diagram of carbon dioxide [24].

Looking at the phase diagram of carbon dioxide as an example (Fig. 3.1), it can be seen that there is a relationship between the pressure and temperature of the vapor in equilibrium with the liquid, as illustrated by the equilibrium curve between the triple point and the critical point. At the pressure and temperature defined by the triple point, all three states of the pure substance coexist in equilibrium. At temperatures below this point, only the solid and gas phases are in equilibrium, while the presence of a thermodynamically stable liquid phase is impossible [2].

If the temperature is increased above the triple point, the density of the liquid phase will start to decrease, while the density of the gas phase will increase, and with it the vapor pressure. The increase in pressure and the change in density of the phases continue until the critical point, at which point the densities of the gas and liquid become equal, the interface between them disappears, and a new single supercritical fluid is formed.

3.2.1 Working near the critical point

In the vicinity of the critical point, the thermodynamic and transport properties of the fluid behave abnormally. Physical properties are still continuous, but their derivatives are not. They may be of opposite sign around the critical point and in many cases tend to infinity. As a result, chromatographers should avoid the critical point and its vicinity during analytical measurements, although in practice, it is almost impossible to accurately set a fluid to its very critical point and perform measurements there.

Tarafder et al. thoroughly discussed the properties of mobile phases in SFC and the effects of working in the vicinity of the critical point in a series of papers [25–30]. They agreed, that the most important chromatographic properties, the retention factor and column efficiencies are related to the density of the mobile phase. However, they also added, that these key parameters depend primarily on the diffusivity of the analytes and their solubility, which in turn are controlled by the mobile phase density and moderately the temperature [25]. They recommended the use of isopycnic plots drawn on the pressure-temperature plane in order to better understand and analyze how chromatograms evolve in SFC when the experimental conditions are changed. The plots are constructed of multiple isopycnic lines covering a wide range of densities. Based on the proximity of the isopycnic lines and the critical point, they distinguished three different working zones on the pressure-temperature plane that are relevant to SFC operations [26].

Fig. 3.2 shows an isopycnic plot of carbon dioxide. The solid circle marks the critical point of carbon dioxide. Zone A is practically a subcritical zone, since the

pressure here is higher than the critical pressure, but the temperature is below the critical temperature. Despite the name of SFC, the inability to reach the supercritical state is not a problem, the chromatographic separation is not affected negatively. The only thing that chromatographers should be aware of in this regard is that no phase transition or phase separation should take place during an SFC run.

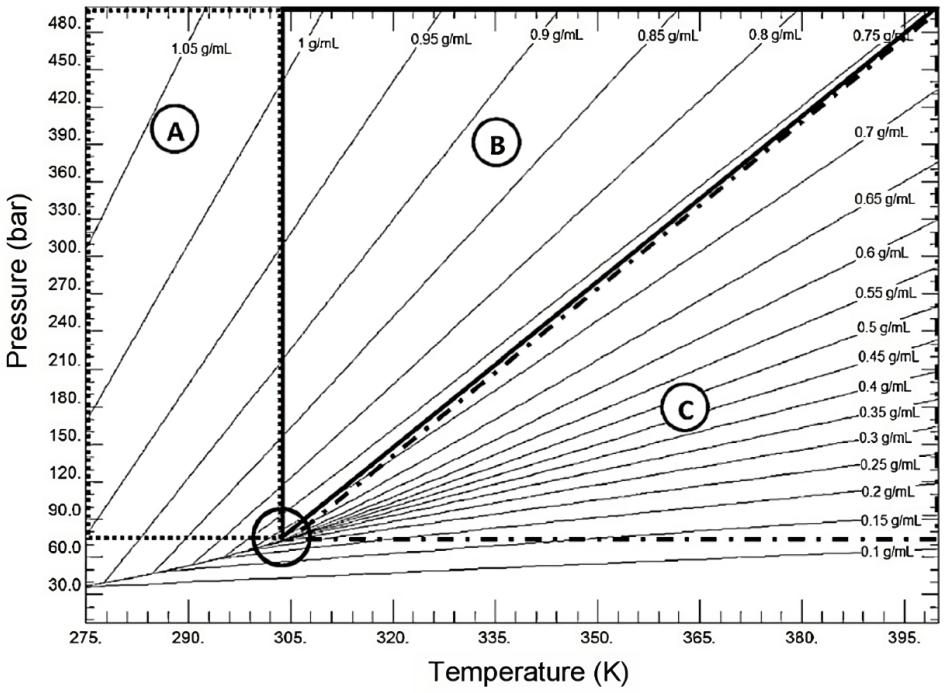

Fig. 3.2: Isopycnic lines ranging from 0.1 to 1.05 g/mL plotted on the pressure-temperature plane of carbon dioxide [26].

In this zone, density does not change too much even with larger steps in pressure. The most notable benefit here is the low compressibility of subcritical CO_2, that makes operation in the zone very similar to working with LC. In addition, the viscosity of carbon dioxide is still lower in this region compared to regular solvents used in LC, that remains true even if organic modifiers are mixed into the mobile phase. This way chromatographers more familiar with LC can easily transfer to subcritical SFC and benefit from higher flow rates and faster analyses provided by the lower viscosity.

Zones B and C mark the supercritical region. The infrequency of isopycnic lines in zone B suggests low compressibility, similarly to zone A, while the densely placed lines in zone C indicate high compressibility. The advantage of zone B over zone A

is that the former enables operating at higher pressures and higher temperatures while maintaining the same density. Operating in zone C offers the most challenges due to the high compressibility of CO_2 here. The primary consequence of this is that even a small pressure drop along the column can induce a significant density gradient, in addition to the quick variation of the thermodynamic properties.

They have also shown that working in the low-pressure section of the supercritical region, in the vicinity of the critical point of carbon dioxide induces a loss of efficiency due to radial thermal heterogeneity inside the column [27]. Early studies identified the pressure drop as the reason behind the decreased efficiency [31]. However, later it was clarified that good chromatographic efficiency can still be reached even with significant pressure drop, if the column outlet pressure is high enough and the difference in density between the inlet and outlet is not too severe [23]. Several chromatographers were able to identify a region of the pressure-temperature plane of carbon dioxide where temperature and pressure are low, and efficiency loss and peak deformations are observed, however, no clear explanation could be given at the time [27].

Berger and Deye theorized that the density gradient alone cannot be blamed for the loss of efficiency, since they could not find a correlation between the efficiency and the density differentials [32]. In addition, the same density differentials at different column temperatures gave different efficiencies. Therefore, they suggested that another parameter related to the temperature could be responsible. Furthermore, it was also observed that in the cases when efficiencies were the lowest, the peaks also exhibited severe fronting. Based on these findings, they suggested that the problem might be a solubility issue and so a mobile phase issue, rather than a column issue.

In a later paper, Berger concluded that at low pressures and temperatures, close to the critical point, a layer of carbon dioxide is adsorbed onto the silica surface of the stationary phase, creating a film with varying thickness depending on the density [33]. The density of the film itself is much higher than that of the density of the mobile phase around it. The thickness of the film is at minimum at high densities of the mobile phase and so retention should be unaffected. However, the film becomes

progressively thicker as the density decreases, creating a larger difference between the densities of the film and the surrounding mobile phase. This thick layer acts as a stationary phase inside the stationary phase, increasing retention severely and preventing chromatographers to perform effective separations, explaining the loss of efficiency. More recent work highlighted that the loss of efficiency and distorted peak shapes were also caused by the formation of radial temperature gradients across the column, induced by the adiabatic expansion of the mobile phase and high pressure drop along the column [34, 35].

These findings led Tarafder et al. to study the thermal effects in detail with the help of the isopynic plots [27]. They concluded that the formation, propagation and decay of thermal effects in the column are controlled by the thermal expansion coefficient and thermal diffusivity of carbon dioxide. They showed that these parameters behave conversely close to the critical point. The thermal expansion coefficient increases rapidly, inducing a fast temperature drop with decreasing density. However, the thermal diffusivity decreases abruptly, reducing the heat transfer ability of the fluid to mitigate the heat difference and reach thermal equilibrium. This contradictory behavior risks the formation of thermal heterogeneity in the column and thus, the loss of efficiency even with low pressure drops along the column.

They also explored the retention behavior of several compounds (octylbenzene, octadecene, anthracene and pyrene) on unmodified and C_{18} bonded silica stationary phases using neat carbon dioxide as the mobile phase [30]. They found that along the isopycnic lines, retention factors decreased steadily with increasing temperature. However, this tendency changed to the contrary near the critical region of carbon dioxide with the retention factors increasing instead with increasing temperature, reaching a maximum and then starting to decrease again. The chemical species of the sample and the stationary phase did not influence the behavior. Three possible reasons were theorized for the phenomenon: (1) the high compressibility of the mobile phase in the critical region; (2) the water content of the mobile phase that could adsorb on the surface of the silica; (3) the formation of multiple layers of

carbon dioxide film on the surface. They concluded that the most probable cause was the heavy adsorption of CO_2 on the stationary phase.

3.2.2 Physico-chemical properties of neat CO_2

After long experimentation of early pioneers with different fluids, carbon dioxide is now the most widely used mobile phase in supercritical separations. It has several advantages: it is inexpensive, non-flammable, available in large quantities of sufficient purity, non-toxic, miscible with organic solvents, has low viscosity and low critical temperature (31 °C) and pressure (73 bar). It is an apolar molecule with a polarity similar to that of n-hexane, making it a good solvent especially for low-polar, medium molecular weight compounds. The density of supercritical carbon dioxide varies between 0.2 and 1.1 g/cm^3, i.e. slightly higher than the density of gases up until the density of liquids [36].

Carbon dioxide is a non-protic solvent, has a low dielectric constant, but has no dipole moment. However, due to the dipoles of the two carbon-oxygen bonds in opposite directions, it has a strong quadrupole moment, which can affect the interactions between carbon dioxide and other molecules. Carbon dioxide is relatively inert, although not completely, as it has been shown to react with platinum catalysts during hydrogenation reactions forming carbon monoxide, that in turn can poison the catalyst [37]. Furthermore, it has been reported that CO_2 can react with secondary amines to form a carbamic acid and an ammonium carbamate salt. Due to its chemical structure, CO_2 can act as a Lewis base on the oxygen atom, pairing with Lewis acids such as phenols and amines, a possible explanation for improved peak shapes in the case of acidic compounds. Depending on the chemical environment, the central carbon atom can acts a Lewis acid due to its partial positive charge [36].

3.2.3 Properties and challenges of binary mixtures

Most samples commonly encountered in chromatographic separation have poor solubility in neat carbon dioxide, leading to high retention and poor selectivity. To overcome this, a more polar organic modifier is mixed to carbon dioxide to increase sample solubility, selectivity and prevent precipitation after sample injection. Most often, low molecular weight alcohols (methanol, ethanol or isopropanol) are used, which interact with the sample components through dipole-dipole interactions or hydrogen bonding.

Binary (and ternary) mobile phases are highly favored due to (1) the increased, adjustable polarity and solvent strength the modifier provides; (2) reducing the effects of remaining silanol groups on the solid support of the stationary phase by blocking active sites; (3) modifying the polarity and characteristics of the stationary phase; (4) assisting the mass transport properties of the mobile phase; (5) adding the ability to perform gradient elution and (6) altering the mobile phase compressibility, density and phase ratio [38, 39]. The inclusion of organic modifiers made SFC into a highly versatile technique capable of covering a wide range of polarities both in terms of normal and reversed phase applications (Fig. 3.3).

Besides organic solvents, additives also made their way to SFC separations at the end of the 1980s, further increasing the polarity of compounds that could be separated [40]. The most common additives mixed into the organic modifier are trifluoroacetic acid, formic acid, diethylamine, triethylamine, ammonium acetate, ammonium hydroxide, ammonium formate, etc. The use of additives have several benefits such as (1) enhancing the solvating power of the eluent; (2) suppressing ionization and forming ion-pairs with charged substances and (3) modifying the surface of the stationary phase by blocking active sites. Additives are a critical necessity in more complex fields of SFC such as chiral separations, where peak shapes and peak integrity can significantly be improved. Water as an additive has been extensively studied by Olesik et al. who also pioneered the fundamental research of enhanced-fluidity liquid chromatography (EFLC), a technique that employs mobile phases composed of large proportions of traditional solvents mixed

with carbon dioxide at subcritical conditions, covering both normal and reversed phases [41–45].

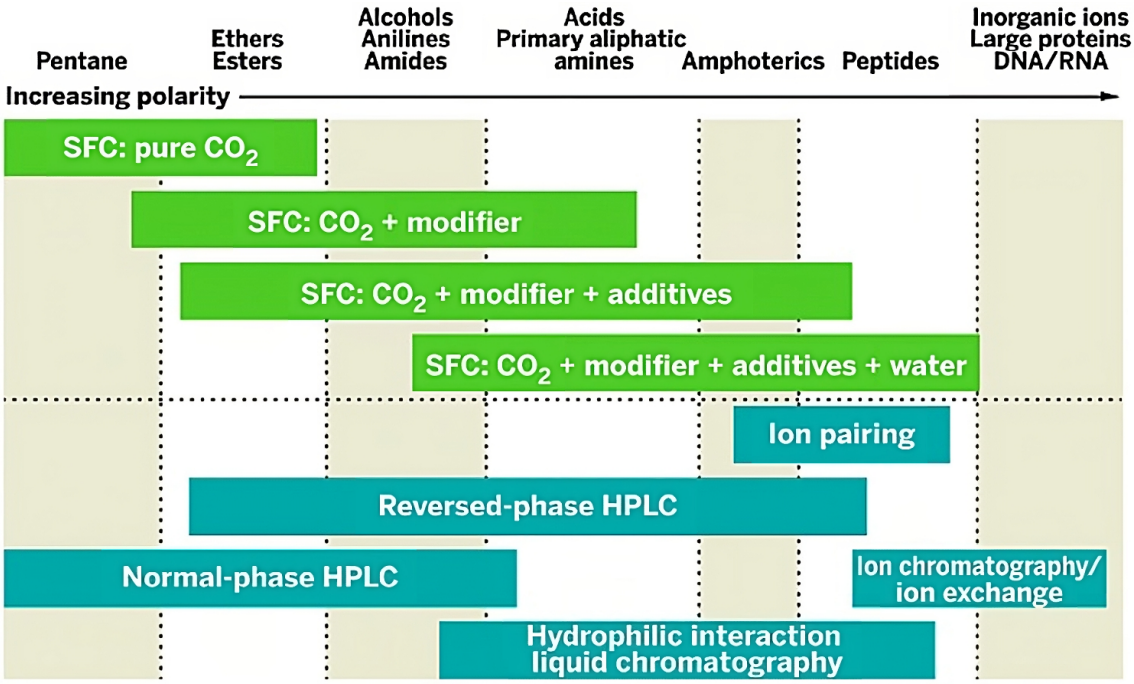

Fig. 3.3: Application range of SFC utilizing organic modifiers and additives compared to conventional LC techniques. The top section denotes the increasing polarity and the types of substances commonly separated [39].

Phase diagrams for mixtures are far more complicated compared to those of pure substances. In addition to pressure and temperature, the equilibrium between the gas phase and the liquid phase is influenced by the composition of the mixture as well as the interactions between the components. A mixture of arbitrary composition will only be in a supercritical state if its pressure and temperature significantly exceed the critical pressure and temperature of the individual components. The groundwork in this field was laid down by van Konynenburg and Scott, who have carried out a detailed study of binary mixtures, providing phase diagrams by solving van der Waals equations of state and creating the nomenclature [46]. The phase diagram of a binary mixture contains the phase diagrams for all possible compositions, including all critical points. The curve connecting the critical points is called the critical curve or critical locus, with the critical points of the two pure substances at the end points (Fig. 3.4). The critical locus may be continuous

(Type I) only in a few cases involving CO_2 and some weakly polar substances with low molecular weights such as light alkanes and alkenes, cyclohexane, toluene, dimethylether, methanol, ethanol, n-propanol, isopropanol, etc. [2]. Mixtures with more complex or polar compounds and CO_2 may undergo phase separation as pressure and temperature increase and their critical locus becomes discontinuous.

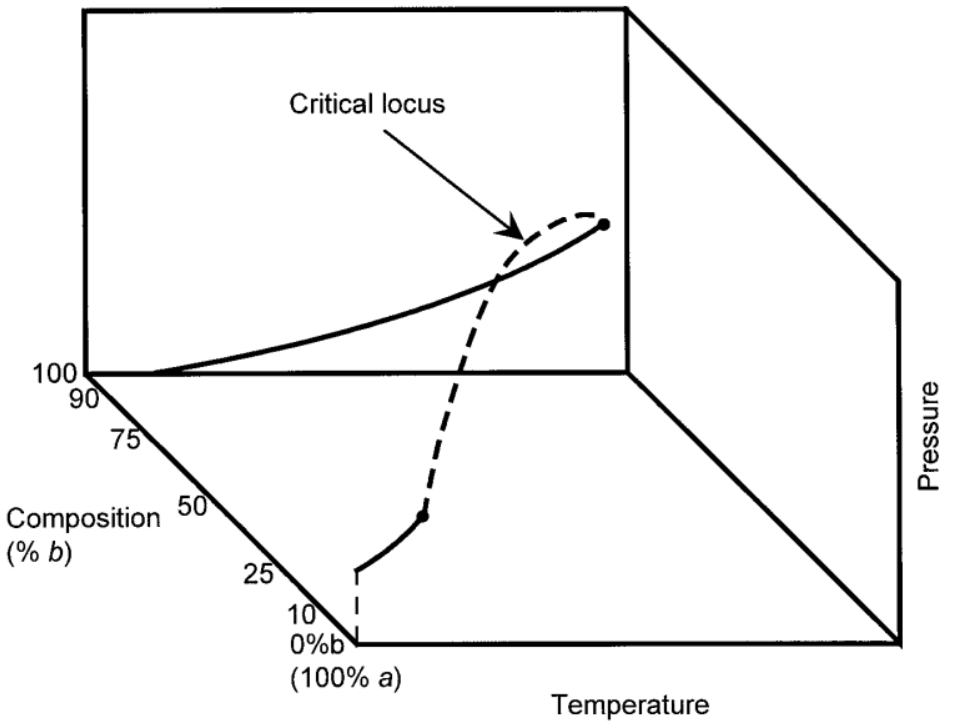

Fig. 3.4: Schematic view of a Type I binary phase diagram with a third axis representing the composition of the mixture. The solid lines represent the boiling lines (the curves between the triple and critical points) of the pure compounds, while the dashed line represents the critical locus, containing the critical points of every composition [47].

The use of binary mixtures is complicated by the complexity of their phase diagrams. If the experimental conditions are not carefully selected, phase separation may occur even in the case of light alcohol modifiers. In this case, the mobile phase splits into gas and liquid phases in equilibrium, both of which separately equilibrate with the stationary phase, leading to changes in the solubility and retention of the components and a noisy baseline due to the gas-liquid mixture entering the detector cell [38]. Fig. 3.5 shows schematic phase diagrams for binary mixtures of CO_2 and methanol at three different temperatures. The diagrams illustrate well how the one-phase and two-phase regions vary as the composition and temperature of mixture

change. The continuous blue boundary lines represent the bubble point and dew point lines. Fig. 3.5a shows the phase diagram at 0 °C, where both components are below their critical temperatures. At this point, the system can only contain either liquid phase or a gas-liquid mixture in dynamic equilibrium. The two phases can coexist in equilibrium if the pressure is between the vapor pressures of methanol (<1 bar) and liquid CO_2 (34 bar) at 0 °C. Fig. 3.5b shows the phase diagram at 100 °C, a temperature higher than the critical temperature of pure CO_2 (31 °C) but lower than that of pure methanol (240 °C). The two-phase region does not cover the entire composition range and the supercritical state of the mixture becomes available given high enough pressure and concentration of CO_2. Fig. 3.5c shows the phase diagram at 200 °C, where the two-phase region is considerably reduced and the supercritical state can exist over a wide composition range [38].

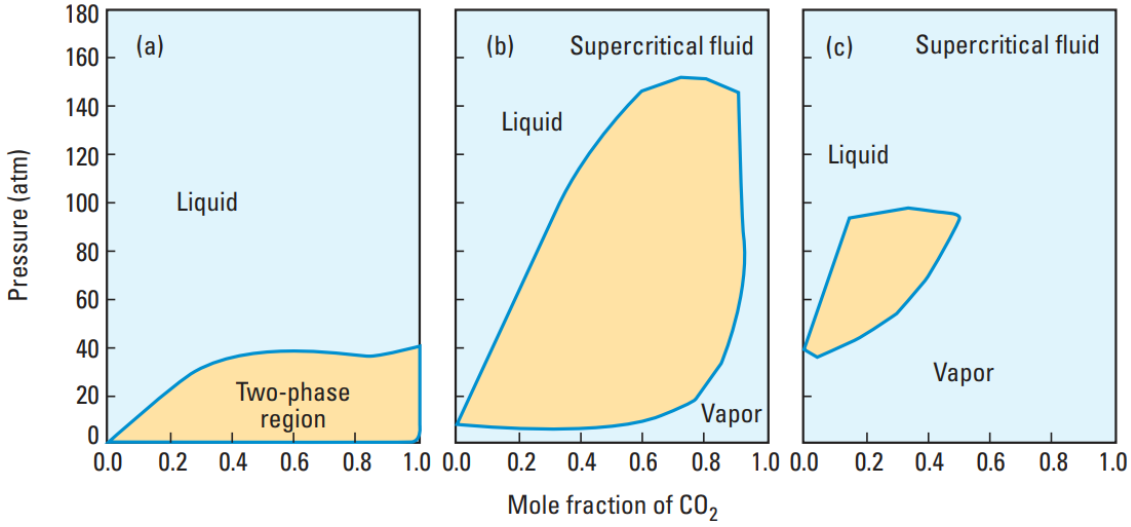

Fig. 3.5: Phase diagrams of CO_2-MeOH binary mixtures at three different temperatures: (a) 0 °C; (b) 100 °C and (c) 200 °C [38].

Fig 3.6 shows an estimation of how the critical conditions of a CO_2-methanol binary mixture changes as a function of the composition. The blue window depicts the most commonly used compositions in SFC applications. At 5% of methanol, the critical pressure of the mixture rises to 105 bar, while the critical temperature is around 51°C. As the methanol content increases, so do the critical conditions. At 30% of methanol, the critical pressure is 168 bar, while the critical temperature is 135 °C. The figure clearly demonstrates how impossible it is to reach supercriticality

in conventional SFC instruments. Even if the system and column would be able to handle the pressure, the temperature requirements are too much for both, as most columns usually have an upper limit up to 60–70 °C.

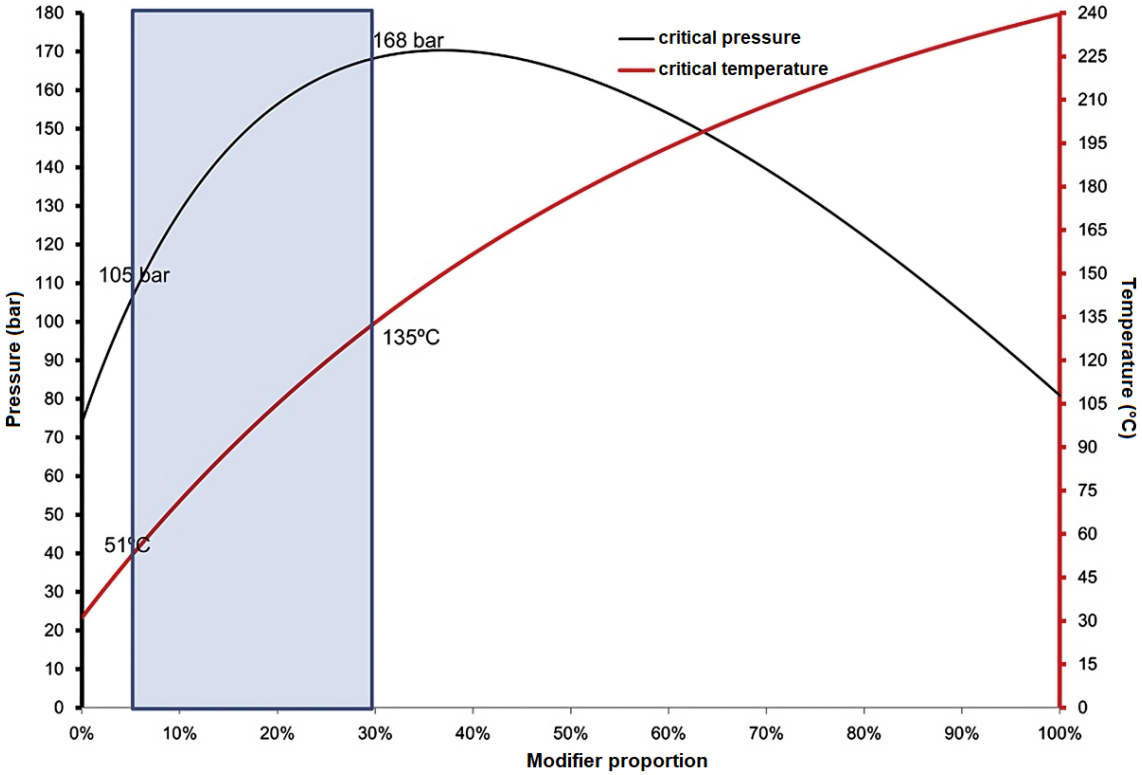

Fig. 3.6: Relationship between the critical conditions and composition for a CO_2-MeOH binary mixture [16].

3.3 Retention anomalies unrelated to the critical region

Recently, Gritti reported unexpected retention phenomena of a series of n-alkylbenzenes in SFC resulting in shifts in retention, band compression and enlargement [48]. The SFC system was highly customized with independent solvent delivery to the injection valve and back pressure regulator, then he also employed a vacuum chamber for the column, custom capillaries for connections and an on-

capillary detection system, all in order to prevent any extra-column band dispersion and the formation of density and thermal gradients in the column.

He found that the sample solvent overloaded the C_{18} column chosen for the study and the solvent band divided the chromatogram into three parts, each with different efficiency results. Analytes less retained than the solvent showed similar column efficiencies as if there was no solvent-analyte band interference. In the case of more retained analytes, decreased column efficiencies were observed due to band enlargement and when both retentions matched closely, the interference resulted in extremely high apparent efficiencies as a result of band compression.

Similar phenomena have been reported for the first time by Nilsson and Westerlund in ion-pair reversed phase liquid chromatography (IP-RPLC) [49]. Besides the analytes, the sample also contained high concentrations of an organic anion that formed ion pairs with a cationic component of the mobile phase. This created a zone with a different composition compared to the bulk mobile phase in the column that induced similar behavior, including band compression, as mentioned above. Other aspects of unexpected retention phenomena was compiled by Lesellier in a recent review [50]. He categorized the uncommon observations depending on whether they were induced by effects related to pressure, temperature or specific interactions between the stationary phase and the chemical structures of the sample.

Choosing the most suitable sample solvent in SFC can be challenging during method development. Naturally, the mobile phase cannot be used since it mainly consists of pressurized carbon dioxide that becomes gaseous at room temperature and atmospheric pressure, therefore a proper liquid has to be selected. Very often the analytes are dissolved in solvents or solvent mixtures imitating the polarity of the mobile phase which the compounds are highly soluble in. Another option is to use the modifier as the solvent. These, however, can lead to solvent-mobile phase mismatches due to solvent strength and viscosity differences that are often detrimental to peak profiles [51]. If neat carbon dioxide without any modifier is used as mobile phase, competition between the solutes and the sample solvent

can also occur for the adsorption sites of the stationary phase that has additional adverse effects on peak integrity [11].

3.4 Adsorption isotherms

Adsorption isotherms describe the relationship between the analytes present in the mobile phase and adsorbed on the stationary phase at equilibrium and constant temperature. In linear chromatography, the relationship is simple, since the equilibrium concentrations of the compounds in the mobile and stationary phases are directly proportional, that is also represented in their isotherm curves. Peak shapes and retention times are independent of the concentration and composition of the sample along with peak heights, which are proportional to the concentration of each compound in the sample [52]. In nonlinear chromatography, however, the relationship is more complex, since the concentrations in the mobile phase and stationary phase are not directly proportional anymore, that gives rise to several difficulties and complicating phenomena. The equilibrium isotherm of a compound is affected by the concentration of all other compounds too. Competition for the adsorption sites can occur with displacement and tag-along effects altering the retention mechanisms.

In order to describe and model the competitive behavior between the analytes and the sample solvent, their single-component equilibrium isotherms have to be determined. The adsorbent surface of the column can be considered nonhomogeneous, thus the different adsorption energy sites need to be accounted for. For this purpose, the bi-Langmuir isotherm was used during the calculations, which is the simplest model for a heterogeneous surface, where the adsorption energy distribution is considered bimodal [52]. The adsorbent surface is assumed to be a combination of two different homogeneous surfaces:

$$q_i = \frac{a_1 C_i}{1 + b_1 C_i} + \frac{a_2 C_i}{1 + b_2 C_i} \tag{3.1}$$

where q_i and C_i are concentrations of component i in the stationary and mobile phases, respectively; a_1 is the initial slope of the isotherm, b_1 the equilibrium constant for one of the sites and a_2 and b_2 are the same parameters for the other site, respectively [52].

The bi-Langmuir isotherm can be extended to multicomponent systems. However, when multiple compounds are present in the sample, they interfere and compete for adsorption. In addition, competition is not limited only to the analytes but can also occur between the sample solvent and the analytes. This is especially true for SFC, where the sample cannot be prepared with the use of the mobile phase. If the surface is nonhomogeneous and the compounds follow bi-Langmuir isotherm behavior then the competition can be described with the competitive bi-Langmuir isotherm as

$$q_i = \frac{a_{i,1}C_i}{1 + b_{\mathrm{A},1}C_\mathrm{A} + b_{\mathrm{B},1}C_\mathrm{B}} + \frac{a_{i,2}C_i}{1 + b_{\mathrm{A},2}C_\mathrm{A} + b_{\mathrm{B},2}C_\mathrm{B}} \tag{3.2}$$

where C_A and C_B are concentrations of component A and B in the mobile phase and the other coefficients are the same as those obtained for the single-component isotherms of the two compounds [52].

3.5 Determination of adsorption isotherms

A number of dynamic methods are available for isotherm determination that can be performed by chromatography. These include the frontal analysis (FA), the elution by characteristic point (ECP), the frontal analysis by characteristic point (FACP), the perturbation method (PM), the retention time method (RTM) and the inverse method (IM) [53, 54]. FA was the most commonly used approach due to its high accuracy, though its main drawback is that it is very time-consuming and resource-heavy. Still, it can be used for competitive isotherm determination, while ECP and FACP are unsuited for this task due to their operating principles and should be used only for rough estimation of the isotherm parameters.

3.5.1 The elution by characteristic point method

Estimation of the initial isotherm parameters can be performed e.g. with the method of elution by characteristic point. In this approach the isotherm is generated from the diffuse rear part of an overloaded band profile, obtained by the injection of a large amount of sample, then integrating the peak area starting from the tail end until the peak maximum that serves as the characteristic point [2]. The isotherm can be calculated using partial sums as follows:

$$q(C) = \frac{1}{V_\mathrm{a}} \int_0^C (V_\mathrm{R} - V_0) \mathrm{d}C \tag{3.3}$$

where $q(C)$ is the amount adsorbed on the stationary phase when it is in equilibrium with concentration C, V_a the volume of the adsorbent, V_R the retention volume of the point in the rear part of the profile at concentration C or characteristic point and V_0 the hold-up volume of the column. Each point of the rear profile gives one point of the isotherm, however the method is derived from the ideal model of chromatography which assumes infinite rate of mass transfer in the column due to constant equilibrium of the mobile and stationary phases, but zero axial dispersion, hence infinite column efficiency. Therefore, the estimation is only applicable with highly efficient columns. In addition, the model assumes rectangular injection profiles, but the resulting error can be decreased by injecting small amounts [55]. Another source of systematic error can be caused by the selection of the starting and ending points of the integration. Although there have been some improvements for ECP that eliminate most of the drawbacks [56, 57], the method was strictly used for rough initial estimation in our study.

3.5.2 The inverse method

The direct problem of chromatography involves calculation of the sample component band profiles with the help of their already known equilibrium isotherms. The inverse problem, on the other hand, involves the determination of the isotherms from the recorded band profiles [53]. The inverse method (IM) is one

of several methods available aiming to solve the inverse problem of chromatography where the column response, the mass balance equation, the initial and boundary conditions are known and the experimental elution profiles are assumed to be solutions of the column model [55].

Unlike most approaches, the isotherm model has to be selected in advance and the initial isotherm parameters are estimated with the help of an analytical injection and another method used in isotherm determination. The next step is the calculation of overloaded band profiles by integration of a chosen mass balance equation. Then the following objective function is used to compare the measured and calculated band profiles:

$$\min \sum_i r_i^2 = \min \sum_i (C_i^{\mathrm{sim}} - C_i^{\mathrm{meas}})^2 \tag{3.4}$$

where C_i^{sim} and C_i^{meas} are calculated and measured concentrations at point i and r_i is their difference. The last step is the minimization of the objective function through the adjustment of the isotherm parameters with the help of an optimization algorithm [53, 54, 58].

The inverse method requires a proper mass balance equation of chromatography in order to work. An accurate mass balance equation can be given with the equilibrium-dispersive (ED) model when mass transfer kinetics are controlled only by very fast molecular diffusion effects. The model assumes constant equilibrium between the mobile and stationary phases, while the band-broadening effects induced by the axial dispersion and the finite rate of mass transfer kinetics are incorporated in an apparent dispersion term. The mass balance equation for each component can be given as:

$$\frac{\partial C_i(z,t)}{\partial t} + F\frac{\partial q_i(z,t)}{\partial t} + u\frac{\partial C_i(z,t)}{\partial z} = D_{\mathrm{a}}\frac{\partial^2 C_i(z,t)}{\partial z^2} \tag{3.5}$$

where z is the distance along the column, t the time, u the mobile phase linear velocity and F the phase ratio determined as:

$$F = \frac{1-\varepsilon_{\mathrm{t}}}{\varepsilon_{\mathrm{t}}} \tag{3.6}$$

where ε_{t} is the total porosity of the column. D_{a} is the apparent dispersion coefficient that can be calculated from an analytical elution profile and is given with:

$$D_{\mathrm{a}} = \frac{uL}{2N} = \frac{Hu}{2} \tag{3.7}$$

where N is the number of theoretical plates and H the plate height. The initial condition

$$C_i(z, 0) = 0 \tag{3.8}$$

states that at $t = 0$ the column is equilibrated with the mobile phase in which the concentration of the solute is zero. The boundary condition (i.e. the injection profile) for each component can be written as:

$$C_i(0, t) = C_i^0 \tag{3.9}$$

$$0 < t \leq t_{\mathrm{p}} \tag{3.10}$$

where t_{p} is the injection time. In some cases, the injection profile may be assumed to be rectangular with a length of t_{p}, although this assumption is incorrect in most practical applications [53, 55]. The inlet profile of the injection has a major effect on band profile and should be known accurately. Therefore, the actual injection profile was obtained from an analytical injection where the column was replaced with a zero-volume connector.

The differential mass balance equation defined in Eq. (3.5) neglects the compressibility of the mobile phase. Therefore, it has limited applicability in SFC where the pressure gradient along the column alters the density of the mobile phase and eventually its elution strength. Nevertheless, when pressure drop along the column is only moderate, Eq. (3.5) gives an accurate estimation of the band profiles.

3.6 The importance of mass flow rate in SFC

A major result of the compressibility of CO_2 is that the actual volumetric flow rate deviates from the set value, in addition to other chromatographic properties being affected as well [2, 59]. Volumetric flow rate is essential for converting retention times into retention volumes, but it is also important for simulations, modeling and other numerical studies. Mass flow rate is considered to be the only flow parameter that stays constant throughout an SFC system [14]. Therefore, it can be utilized very well to determine actual volumetric flow rates by accurate and careful measurements.

Mass flow rate and its interpretation in SFC have been studied extensively in recent years. Tarafder and Guiochon discussed the factors affecting the mass and volumetric flow rates and their variation given by different operating conditions [60]. They pointed out the general lack of information regarding actual flow rates of the mobile phases at the time. Moreover, a detailed report on the importance of these parameters and their accurate determination was provided, supported by a series of systematic simulations performed by an iterative method. Practical implementations were reported by Tarafder et al. in a follow-up paper focusing on the challenges and benefits of proper on-line mass flow measurements with the help of an external Coriolis flow meter [61]. Besides flow rates, the study also pointed out the opportunity of continuous monitoring and diagnosis of correct instrument operation.

Several SFC practitioners are working with CFM instruments to provide more authentic data on true experimental conditions. The research group of Fornstedt thoroughly investigated several topics in analytical and preparative scale SFC, including modifier/additive adsorption, solute retention and chiral separations affected by variations of set vs actual experimental parameters [12, 62–64]. All studies were complemented by in-depth mass flow data for total and modifier volume flow information.

Placement of the CFM in the chromatographic system plays a critical role. Several options are available that can provide additional information regarding

the operation of the individual system units. Placing the flow meter upstream the pump allows for a wider range of operating pressure, but might also result in increased noise of the mass flow signal [61]. Placing the CFM downstream the pump significantly reduces noise and also gives information about possible leaks as well as mass or molar fractions of the mobile phase composition depending on the position around the mixer [12, 62–64]. Placing the instrument around the column gives information about the mass flow more affected by the experimental conditions. Since the CFM is downstream the injection module in this setup, disturbances can be observed in mass flow during experiments that are related to the sample being injected into the mobile phase stream. Accounting for the fluctuations can produce more accurate results, especially for sample components with lower retention factors and for hold-up time markers [65].

Mass flow rate is very closely connected to pressure, temperature and density that have been extensively studied by chromatographers [66–68]. Although research focusing on neat carbon dioxide mobile phases and the role of mass flow rate is limited, the information gathered from a detailed study on these topics should be useful for reliable measurements of retention factors for robust method transfer and scale-up from analytical to preparative SFC, that is more mass-controlled [69], and ultra-high performance SFC (UHPSFC), where robustness suffers from larger changes in parameters [70, 71].

3.7 The importance of hold-up volume and hold-up time in SFC

Hold-up volume and hold-up time determination have been a cardinal problem in SFC. The hold-up or void volume is a key parameter in many areas, including retention mechanisms, mass transfer kinetics, modeling purposes or isotherm determination. Several methods are available in LC that have been studied and adapted to SFC with more or less success [59, 72–75]. These methods can be divided into two groups, static methods and dynamic methods. Static methods aim to determine the column void volume outside of the chromatographic instrument. The most commonly used method in this category is the gravimetric or weight-difference method, which consists of first evacuating all traces of previous solvents from the column, weighing it, then saturating it with solvents of known densities and then weighing again. The difference of the two masses can be used to calculate the hold-up volume. The main disadvantage of this method is that it does not consider the solvation and elevated pressures of the chromatographic environment. Dynamic methods employ the chromatograph to calculate the hold-up volume. The methods include the minor disturbance method, inverse size-exclusion chromatography (ISEC) and the injection of an unretained marker.

Unretained markers offer the fastest method and are the most commonly used approach to measure the hold-up time, which then can be used for void volume determination if additional requirements, related to the mass flow rate and volumetic flow rate are met. Previously, the first negative shift of the baseline, system peaks, solvent peaks, minor disturbance peaks or compounds considered unretained have been used for hold-up time measurements [12, 14, 55, 63, 76], while in chiral SFC, acetone or 1,3,5-tri-*tert*-butylbenzene (TTBB) proved to be reliable hold-up time markers [77, 78]. Guardale et al. studied and compared several methods for void volume determination in SFC, including the gravimetric method, the homologous series linearization method and the unretained marker method, with acetronitrile, tetrahydrofuran, acetone and heptane as potential markers. They concluded that acetonitrile as unretained marker was the best choice

for their studies with C_{18} columns and a wide range of mobile phases, since the other compounds were either retained or could not produce satisfactory signals [72].

The use of nitrous oxide (N_2O) as a hold-up time marker for SFC has been established for a decade now with the first applications reported by Vajda et al. in 2013 [59, 65, 73]. Nitrous oxide displays beneficial properties that make it an ideal hold-up time marker such as low to negligible adsorption on the stationary phase, low dipole moment, high vapor pressure and low concentration required that prevent any competition with other mobile phase components for the adsorption sites while also providing well-resolved peaks. Sample preparation is simple due to the relatively good solubility of the gas in alcohols. Since its introduction, nitrous oxide has been used extensively as a hold-up time marker in SFC, especially by the research group of Fornstedt [11, 51, 64, 77].

4

Materials and methods

4.1 Instruments

The experiments were performed using a Waters ACQUITY UPC^2 system (Milford, MA, USA). The instrument was equipped with a binary solvent delivery pump, an autosampler with a 10 μL sample loop, a column thermostat, a photodiode array (PDA) detector and a back pressure regulator. The instrument was controlled by the Empower 3 chromatography data software. The extra-column volume of the instrument was 60 μL from the loop to the detector cell and was measured by replacing the column with a zero-volume connector. All retention volumes were corrected for this contribution. Multiple dynamic leak tests were performed for the CO_2 and solvent pumps to verify they are not leaking. Both the accumulator and primary heads passed the tests.

Some experiments were performed using an Agilent 1260 Infinity II SFC System equipped with a binary pump, multisampler, multicolumn thermostat, diode array detector (DAD) and SFC control module. The instrument was controlled by the Agilent ChemStation software.

Mass flow rate of the mobile phase was measured with a mini CORI-FLOW mass flow meter from Bronkhorst High-Tech B.V. (Ruurlo, Netherlands), Model No. M13-ABD-11-0-S, Serial No. B11200776A. This model provides an accuracy of ± (0.2% of the read value + 0.5 g/h), expressed as a sensitivity of 0.01 g/min of CO_2.

The calibration of the mass flow meter was verified by disconnecting CO_2 from the binary solvent delivery system, then pumping water through the CFM at 0.50, 1.00 and 1.50 mL/min set flow rates for 5 minutes at room temperature and collecting the water in a pre-weighed container. If the calibration is correct and the solvent pump delivers accurately, then the CFM readings for the mass flow

rate should be (volumetric flow rate, mL/min) $\times$ (solvent density, g/mL) and the collected mass in the vial should be (volumetric flow rate, mL/min) $\times$ (collection time, min) $\times$ (solvent density, g/mL). The calibration results are summarized in Table 4.1.

Table 4.1: Results of the calibration studies performed with the CFM.

	$F_{\mathrm{v,set}}$ (mL/min)		
H_2O (g)	0.50	1.00	1.50
1	2.4735	4.9526	7.4664
2	2.4730	4.9579	7.4667
3	2.4416	4.9566	7.4659
$\bar{m}$ (g)	2.4627	4.9557	7.4663
$\bar{V}$ (mL)	2.4700	4.9704	7.4884
$m_{\mathrm{exp,25°C}}$ (g)	2.4926	4.9852	7.4779
error (%)	1.20	0.59	0.15
$F_{\mathrm{m,meas}}$ (g/min)	0.50	0.99	1.48
$F_{\mathrm{v,25°C}}$ (mL/min)	0.494	0.994	1.498
	(1.20%)	(0.59%)	(0.15%)
$F_{\mathrm{v,32°C}}$ (mL/min)	0.503	0.995	1.487
	(0.50%)	(0.50%)	(0.84%)
$F_{\mathrm{v},\rho\mathrm{CFM}}$ (mL/min)	0.501	0.993	1.485
	(0.20%)	(0.67%)	(0.97%)

Table 4.2: Densities at 25 and 32 °C and those measured by the CFM at different mass flow rates.

T (°C)	ρ (g/cm^3)
25	0.997047
32	0.995002
$F_{\mathrm{m,meas}}$ (g/min)	
0.50	0.9980
0.99	0.9967
1.48	0.9963

$F_{\mathrm{v,set}}$ denotes the set volumetric flow rates at which the water was pumped. The average volume ($\bar{V}$) was calculated from the average mass ($\bar{m}$) of the collected water and its density at room temperature (Table 4.2). The expected mass of water ($m_{\mathrm{exp,25°C}}$) was calculated as stated above. The error shows the discrepancies between the average mass ($\bar{m}$) and the expected mass ($m_{\mathrm{exp,25°C}}$). $F_{\mathrm{m,meas}}$ denotes the measured mass flow rate. Based on these results, it was concluded that the calibration of the flow meter is accurate and the solvent pump is delivering the correct volume.

It is important to note that the CFM operates at elevated temperatures, likely due to frictional, mechanical and electrical sources. Its software revealed that the temperature inside the flow cell was 32 °C when operated with water. Therefore, volumetric flow rates for 25 ($F_{\mathrm{v,25°C}}$) and 32 °C ($F_{\mathrm{v,32°C}}$) were also calculated using densities shown in Table 4.2. In addition, the CFM recorded different densities at different set flow rates at its operating temperature, so volumetric flow rates were calculated using those densities too ($F_{\mathrm{v},\rho\mathrm{CFM}}$). The values in brackets show the discrepancies between the set and calculated volumetric flow rates.

Pressure values at the inlet and outlet of the column were recorded using a DPG4000 external pressure gauge from OMEGA Engineering (Norwalk, CT, USA).

4.2 Chemicals

Carbon dioxide ($\geq$ 99.5%) was purchased from Linde (Répcelak, Hungary). HPLC grade benzene ($\geq$ 99.5%), acetonitrile ($\geq$ 99.9%), methanol ($\geq$ 99.9%), hexane ($\geq$ 95%) and heptane ($\geq$ 99%) were purchased from VWR International (Fourtenay-sous-Bois, France) and Fisher Scientific (Loughborough, UK).

The analytical standards ($\geq$ 99%) ethylbenzene, butylbenzene, hexylbenzene (97%), octylbenzene, decylbenzene, dodecylbenzene, tetradecylbenzene and octadecylbenzene were all purchased from Sigma-Aldrich (Steinheim, Germany). Nitrous oxide (99%) was purchased from Messer (Lenzburg, Switzerland). 1,3,5-tri-*tert*-butylbenzene (97+%) was purchased from ThermoFisher GmbH (Kandel, Germany). Trifluoroacetic acid (TFA, $\geq$ 99%) was also purchased from Sigma-

Aldrich (Steinheim, Germany). Acetone (distilled) was provided in-house by the Department of General and Inorganic Chemistry (University of Pécs, Hungary).

4.3 Columns, experiments and calculations

4.3.1 Competitive adsorption studies

In the early stages of the competition studies, several stationary phases were tested for uncommon retention behavior. The columns involved were Zorbax Eclipse Plus C18, SB-C8 and C18 (3.5 μm, 4.6 × 150 mm) from Agilent Technologies (Palo Alto, CA, USA), Synergi MAX-RP (4 μm, 4.6 × 150 mm) from Phenomenex (Torrance, CA, USA), Ascentis Express C18 (2.7 μm, 2.1 × 50 mm) and Kromasil C18 (5 μm, 4.6 × 150 mm) from Sigma-Aldrich (St. Louis, MO, USA), and lastly Symmetry C8 and C18 (3.9 and 4.6 × 150 mm, respectively) from Waters.

Eventually, a 4.6 × 150 mm Supelcosil ABZ+Plus alkylamide column packed with 3 μm particles from Sigma-Aldrich was chosen for further studies. The total volume of the column was $V_{\mathrm{tot}} = 2.492$ cm^3. The void volume was estimated by two methods, the weight-difference method, that usually gives an underestimation, and with the help of heptane used as an unretained marker [59]. Both approaches gave very similar results so $V_0 = 1.590$ cm^3 was used in the end. The total porosity was calculated to be $\varepsilon_{\mathrm{t}} = 0.638$, calculated as follows:

$$\varepsilon_{\mathrm{t}} = \frac{V_0}{V_{\mathrm{tot}}} \tag{4.11}$$

Calculations of the mobile phase densities were based on the column thermostat temperature and the inlet and outlet pressures of the column measured directly using the external pressure gauge. The densities were calculated using the National Institute of Standards and Technology (NIST) REFPROP database.

The mean volumetric flow rate ($\bar{F}_{\mathrm{v}}$) was estimated from the measured mass flow rate of the mobile phase recorded downstream the mixer and the average

density ($\bar{\rho}$), calculated as the arithmetic mean of the densities at the inlet and outlet of the column as follows:

$$\bar{F}_{\mathrm{v}} = \frac{F_{\mathrm{m,meas}}}{\bar{\rho}} \tag{4.12}$$

However, individual volumetric flow rates for the inlet and outlet of the column can also be calculated. Based on the measured data, the volumetric flow rate at the inlet was $F_{\mathrm{v,in}}$ = 1.16 mL/min and $F_{\mathrm{v,out}}$ = 1.20 mL/min at the outlet at 60 °C temperature and 150 bar back pressure. The reason for these specific experimental conditions is explained later in Section 5.1.1. The difference in volumetric flow rates is interesting but not unexpected. Because of the adiabatic expansion of carbon dioxide along the column, a higher mobile phase velocity at the outlet of the column can be expected.

It has been shown that there is a difference between set and actual experimental parameters in SFC. However, in the case of moderate temperatures, the column thermostat setting can be a good approximation of the actual conditions [55, 62]. At the time of the experimental work, no temperature sensors were available for accurate measurements at the column inlet and outlet, therefore accuracy of the temperature data could not be determined. The column was equilibrated for 60 minutes at every set temperature in order to introduce the smallest error possible to the model.

The chromatographic measurements during the competitive adsorption studies were carried out with 100% CO_2 mobile phase. The volumetric flow rate was set at 1.00 mL/min, the actual flow rate was calculated to be 1.18 mL/min at 60 °C and 150 bar back pressure. The column temperature was varied between 35 and 60 °C, the back pressure regulator was set at either 105, 150 or 200 bar. The injection volume was 2.0 μL. The detector signal of the alkylbenzenes was recorded between 190 and 400 nm, the optimal channels were 260 and 273 nm.

The samples contained benzene, ethylbenzene, butylbenzene, hexylbenzene, octylbenzene, decylbenzene, dodecylbenzene, tetradecylbenzene and octadecylbenzene dissolved in either acetonitrile, methanol or heptane. The concentrations were set at 0.5, 0.7, 1.1, 1.8, 2.2, 3.4, 4.5, 5.0 and 5.4 g/L, respectively.

During the evaluation of the results, column efficiency was characterized by the number of theoretical plates or plate count, acquired by fitting exponentially modified Gaussian functions (EMG) to the experimental data. The fitting was performed in PeakFit v4.12 software. The EMG function is the most commonly used asymmetrical model for describing peak profiles in linear chromatography, that also considers extra-column band broadening effects [79]. These effects can arise from multiple sources in a chromatographic system. For example, any volume present in connections and fittings can increase the peak width and asymmetry. If the injected sample travels in a smooth manner, then Gaussian-type band broadening can be observed in tubings. However, any volume where mixing takes place usually introduces exponential tailing contribution to the profile. The EMG peak profile can be written as follows:

$$y(t) = \frac{A_{\mathrm{T}}}{2\tau} \exp\left(\frac{\sigma^2}{2\tau^2} - \frac{t - t_{\mathrm{R}}}{\tau}\right)\left[1 - \mathrm{erf}\left(\frac{\sigma}{\sqrt{2}\tau} - \frac{t - t_{\mathrm{R}}}{\sqrt{2}\sigma}\right)\right] \tag{4.13}$$

where A_{T} the peak area, τ a time constant, σ the standard deviation and t_{R} the retention time.

After fitting EMG functions to the experimental data, the plate count values were calculated using the first absolute moment (μ_1), that refers to the mean or average retention time, and the second central moment (μ_2'), that refers to the variance of the peak, as follows:

$$\mu_1 = t_{\mathrm{R}} + \tau \tag{4.14}$$

$$\mu_2' = \sigma^2 + \tau^2 \tag{4.15}$$

$$N = \frac{\mu_1^2}{\mu_2'} \tag{4.16}$$

Linear detector calibration was performed in order to convert absorbances into concentration, that is necessary if we want to use the equilibrium-dispersive

model of chromatography. By integrating the elution profile, the amount of the injected sample (m_{inj}) can be obtained as follows:

$$m_{\mathrm{inj}} = \int C(V)\mathrm{d}V = \bar{F}_{\mathrm{v}} \int C(t)\mathrm{d}t \tag{4.17}$$

Absorbance at any given time ($A(t)$) is proportional to concentration in the linear range of the detector signal. The relation can be expressed with a sensitivity factor (κ) as follows:

$$A(t) = \kappa C(t) \tag{4.18}$$

$$A_{\mathrm{T}} = \int A(t)\mathrm{d}t = \kappa \int C(t)\mathrm{d}t = \frac{\kappa m_{\mathrm{inj}}}{\bar{F}_{\mathrm{v}}} \tag{4.19}$$

$$\kappa = \frac{A_{\mathrm{T}} \bar{F}_{\mathrm{v}}}{m_{\mathrm{inj}}} \tag{4.20}$$

With κ determined, concentration is easily obtained as:

$$C(t) = \frac{A(t)}{\kappa} \tag{4.21}$$

4.3.2 Mass flow studies

During the mass flow studies, two columns were utilized, a Spherisorb Silica column (5 μm, 4.6 × 100 mm) from Waters and the Supelcosil ABZ+Plus alkylamide column (3 μm, 4.6 × 150 mm) from Sigma-Aldrich. The idea behind the column selection was to use different stationary phase chemistries, structures and dimensions in the hopes of finding more varied results due to different thermodynamic environments forming inside the columns. All experiments were performed with a 100% CO_2 mobile phase with a set volumetric flow rate of 1 mL/min. The injection volume was 2.0 μL, the detector signal was recorded between 190 and 400 nm. Four different sets of settings were used for the column thermostat and back pressure regulator as shown in Table 4.3.

Total mass flow rates and pressures were measured directly at the inlet and outlet of the column also in four different configurations as shown in Fig. 4.1. During the data acquisition, all instruments were brought to an equilibrium, then

Table 4.3: The four sets of settings for the column thermostat and back pressure regulator.

	T (°C)	p (bar)
A	20	104
B	20	150
C	40	104
D	40	150

an injection of hexane was made. The chromatograms were recorded for 3 minutes, during which the CFM signal was recorded as well, consisting of the mass flow, density and temperature profiles of the eluent passing through the CFM cell. Three replicate measurements were performed for the four sets of settings (A through D), the four configurations (I through IV) and the two columns as well as a zero-volume union.

Hold-up time measurements were performed with the same experimental conditions and columns but without the CFM and pressure gauge installed. Nitrous oxide was selected as the hold-up time marker. The gas was bubbled through methanol for one minute then the solution was injected in three replicate measurements. Detection wavelengths were 195 and 200 nm.

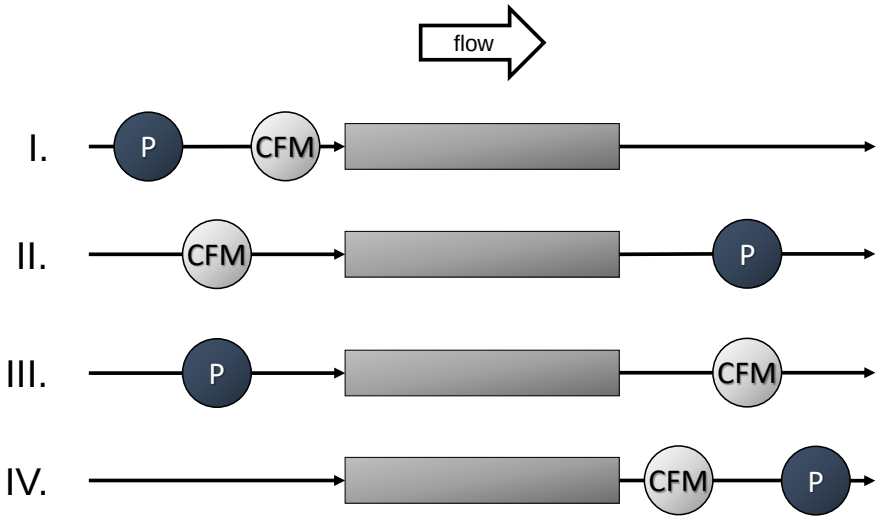

Fig. 4.1: Schematic view of the four configurations of the CFM and pressure gauge (P) around the inlet and outlet of the column.

Extra-column volumes and variances with and without the CFM installed were determined by disconnecting the column, the CO_2 pump and the back pressure regulator. Then three replicate injections were performed using 70/30 MeOH/H_2O mobile phase with a volumetric flow rate of 0.25 mL/min. EMG functions were fitted to the experimental profiles and extra-column volumes and variances were calculated using the first absolute moment and the second central moment, respectively. The volume with no CFM (and pressure gauge) installed was 60 μL and the variance was 406 μL^2. With the CFM connected, the volume was 2.06 mL and the variance was 1.67 mL^2, so the volumetric contribution of the CFM was 2.00 mL.

4.3.3 Hold-up time studies

The columns employed in the hold-up time studies were two Spherisorb Silica columns (5 and 10 μm, 4.6 × 100 mm), a Symmetry C18 (3 μm, 4.6 × 150 mm), a Viridis BEH (1.7 μm, 3.0 × 50 mm) and a Torus Diol (1.7 μm, 3.0 × 50 mm), all from Waters along with the Supelcosil ABZ+Plus alkylamide column (3 μm, 4.6 × 150 mm) from Sigma-Aldrich and a (S,S) Whelk-O1 (4.6 × 100 mm), packed with fully porous, 1.8 μm particles synthesized at the Department of Chemical, Pharmaceutical and Agricultural Sciences (University of Ferrara, Italy) [80].

The experiments were performed with a set volumetric flow rate of 1 mL/min. The samples and mobile phases are specified in each corresponding section of Chapter 5. The injection volume was 2.0 μL. The detector signal was recorded between 190 and 400 nm. Four different sets of settings were used for the column thermostat and back pressure regulator as shown in Table 4.3.

5 Results and discussion

5.1 Modeling the competitive adsorption of the sample solvent and solutes

In this sections, our findings related to the uncommon retention behavior studies of n-alkylbenzenes are discussed. First we investigated whether the sample solvent had any detrimental effect on retention. Then, single-component adsorption isotherms were calculated to obtain the isotherm parameters. Lastly, we constructed competitive isotherms to model the competitive behavior of the sample solvent and solutes with the real compounds and two hypothetical ones.

5.1.1 The effect of different sample solvents

Screening measurements for all stationary phases were performed with the three different samples containing either acetonitrile, heptane or methanol as solvent. The purpose of the experiments was to find well-detectable solvent adsorption that had an effect on the retention mechanism of the analytes with neat carbon dioxide mobile phase. In the case of acetonitrile and heptane, no such phenomenon could be identified on any of the columns.

Methanol, however, overloaded the alkylamide column and exhibited a strong, easily detected adsorption. By adjusting temperature and pressure, the relative retention of the solvent and the analytes was influenced in a way that the chromatogram would be divided into two parts around the middle. This was achieved with 60 °C temperature and 150 bar back pressure. Fig. 5.1 shows the experimental chromatograms obtained in methanol (top) and heptane (bottom).

The top graph shows a well-defined band of methanol starting at around $t = 2.65$ min that was confirmed by single injections of the solvent.

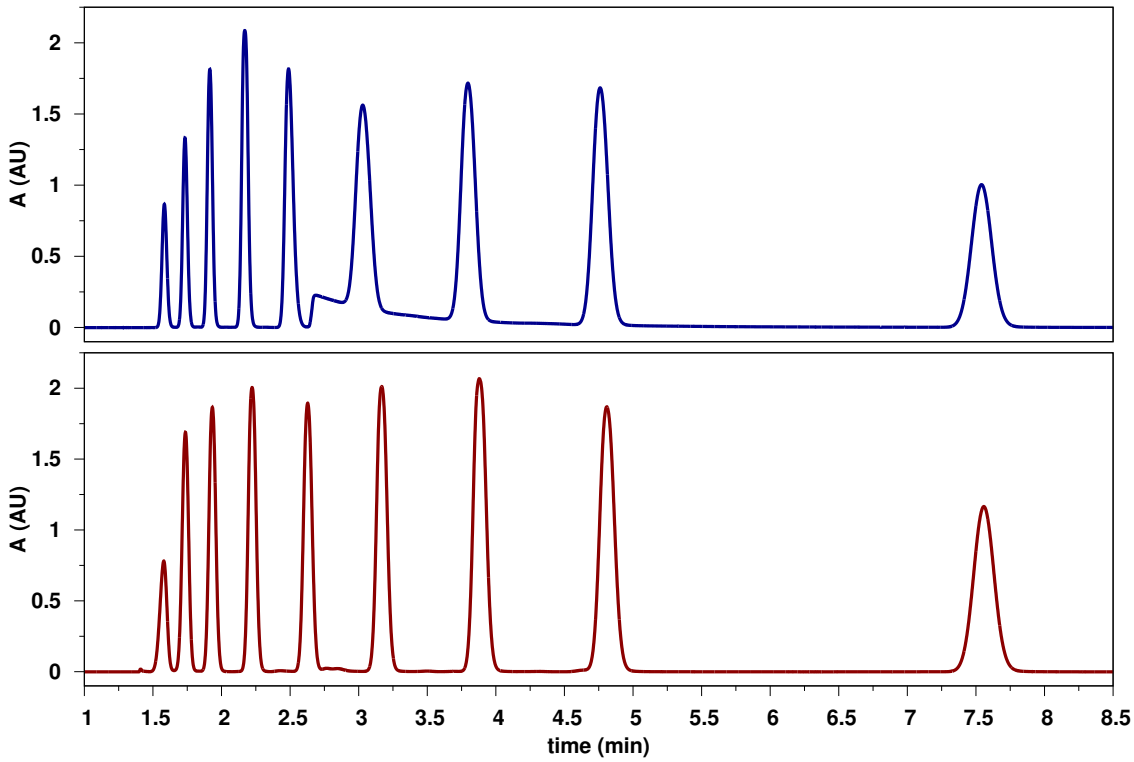

Fig. 5.1: Chromatograms of n-alkylbenzenes in methanol (top) and heptane (bottom) obtained with the alkylamide column, neat CO_2 mobile phase, 200 nm, 60 °C and 150 bar back pressure.

Comparing the two chromatograms, the changes in column efficiency, retention times and peak widths are rather distinct and are caused by competitive adsorption of methanol and the alkylbenzenes for the adsorption sites. When the sample is dissolved in heptane, it can be observed that the number of theoretical plates continuously increases along the homologous series (Fig. 5.2). When the sample solvent is methanol, however, a significantly larger efficiency is observed for homologues smaller than octylbenzene compared to the efficiency when heptane is the sample solvent.

This is caused by the displacement effect that the large amount of methanol induces; as methanol displaces the alkylbenzenes, a peak focusing or sharpening is observed. Then, for the later eluting alkylbenzenes, the efficiency suddenly drops due to the tag-along effect induced again by methanol. The retention time

of octadecylbenzene is large enough so the efficiency for that compound is not disturbed by the adsorption of the sample solvent methanol.

A closer look on efficiency (Fig. 5.2) and retention times (Fig. 5.3) further supports the assumption and shows that the most affected compounds were around the maximum of the methanol band, namely octylbenzene and decylbenzene. Accordingly, further calculations and simulations focused on this section of the chromatogram.

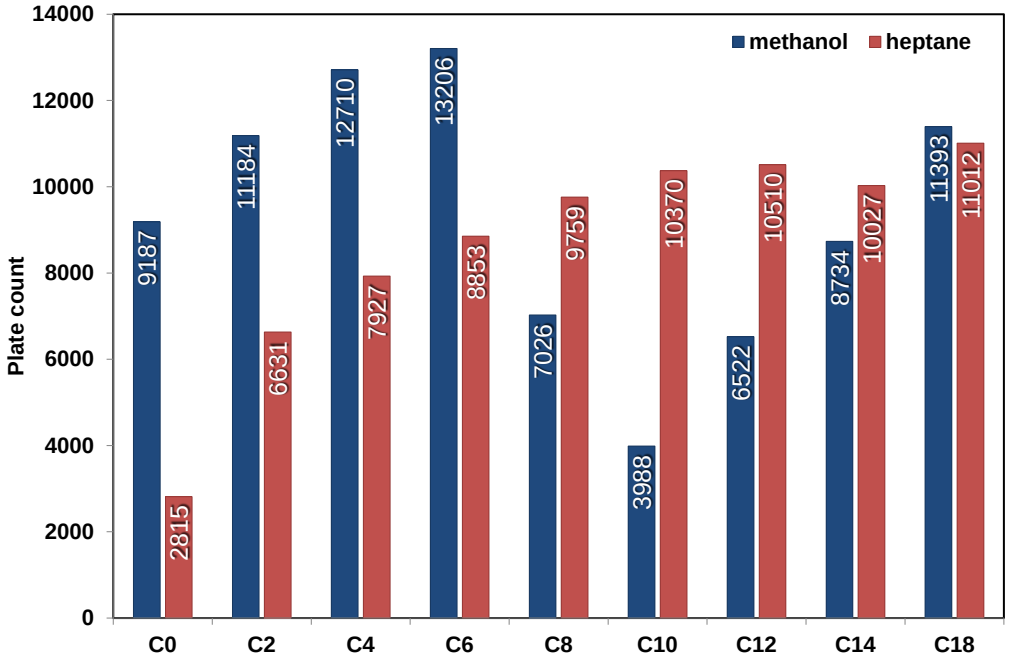

Fig. 5.2: Column efficiencies for each alkylbenzene (C_0–C_{18}) in the case of the two sample solvents, methanol and heptane. The negative effect of methanol is prevalent in the case of octylbenzene, decylbenzene and dodecylbenzene, while compounds eluting earlier showed increased efficiency due to band compression.

5.1.2 Single-component isotherms

Overloaded band profiles of methanol, octylbenzene and decylbenzene were recorded for the purpose of determining the single-component isotherms by the inverse method. The two alkylbenzenes could not be properly dissolved in methanol to obtain a sample with high enough concentration, so injections of the neat standards were performed instead. Calculations required concentration profiles rather than the original, absorbance versus time profiles, therefore calibration of the

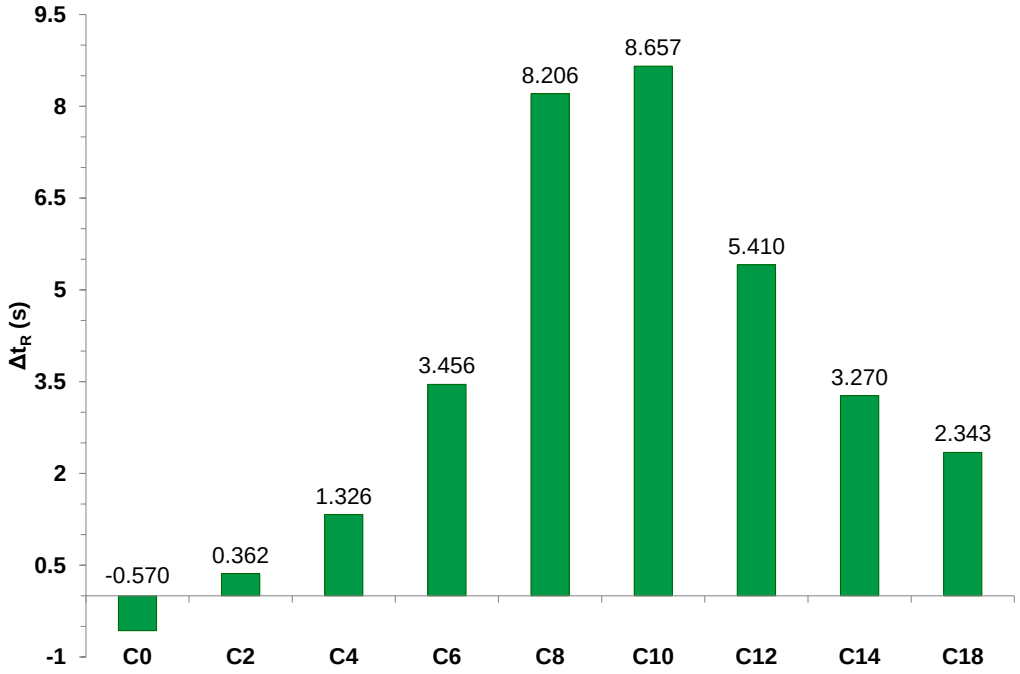

Fig. 5.3: Shifts in retention times in the case of methanol, where the chromatogram obtained in heptane was used as reference for the calculation. Positive values mean a decrease in retention time in seconds. The results for benzene should be disregarded due to its very low retention resulting in a close proximity to the system peaks.

detector was necessary. We chose a linear calibration approach, so the wavelength of 273 nm was selected for the recorded chromatograms of alkylbenzenes to remain in the linear range of the detector response. Absorbances of methanol, octylbenzene and decylbenzene were transformed into concentrations. The steps of calibration are detailed in Section 4.3.1, Equations (4.17–4.21).

The initial isotherm parameters were estimated numerically with the ECP method. The algorithm calculated isotherm curves from the diffuse rear parts of the chromatograms as well as the void and adsorbent volumes of the column. The parameters were obtained by fitting the bi-Langmuir isotherm on the output curves.

The inverse method was applied to the overloaded band profiles of the three compounds to accurately determine their single-component adsorption isotherms. The calculations were performed by a numerical method where the differential mass balance equation given by the ED model was integrated by a modified Rouchon algorithm, ignoring the empty sections of the (z, t) plane to speed up calculations. The method employed a nonlinear simplex algorithm to determine the isotherm

parameters. Besides the overloaded profiles, the initial isotherm parameters and the column parameters, the method also required the inlet profile of the injection that was recorded with a zero-volume connector.

The measured and calculated profiles are plotted in Fig. 5.4. The calculated data fits very well to the experimental profiles confirming the bi-Langmuir model was an appropriate choice for the heterogeneous surface with bimodal adsorption energy distribution. Table 5.1 summarizes the final isotherm parameters for the three compounds. The final sum of squared residuals (FSSR) is a measure of the variance of the fitting error that gives information about the goodness of the fit. The values further support the observations of Fig. 5.4. The two adsorption sites, characterized by saturation capacities $q_{\mathrm{s},1}$ and $q_{\mathrm{s},2}$, respectively, showed similar behavior in all cases. All compounds exhibited a stronger affinity to site 1 during the adsorption process while site 2 was saturated early on.

Table 5.1: Single-component isotherm parameters determined by the inverse method

	methanol	octylbenzene	decylbenzene
a_1	2.652	0.828	1.521
b_1 (L/g)	0.181	0.003	0.004
$q_{s,1}$ (g/L)	14.671	317.222	374.596
a_2	3.895	0.833	0.890
b_2 (L/g)	4.885	0.024	0.024
$q_{s,2}$ (g/L)	0.797	34.736	37.579
FSSR	0.661	2.947	2.919

The isotherm curves along with the curves of the individual sites are plotted in Fig. 5.5. The large amount of the strongly adsorbing methanol resulted in site 2 reaching its maximum saturation capacity very quickly. Interestingly, the two alkylbenzenes did not really enter the nonlinear range of the isotherm, so the curves give only an approximation of the adsorption phenomena. These observations can be explained with the injected amounts, containing only the neat compounds, undergoing a quick and severe dilution immediately after entering the column resulting in a two orders of magnitude decrease in concentration along the column.

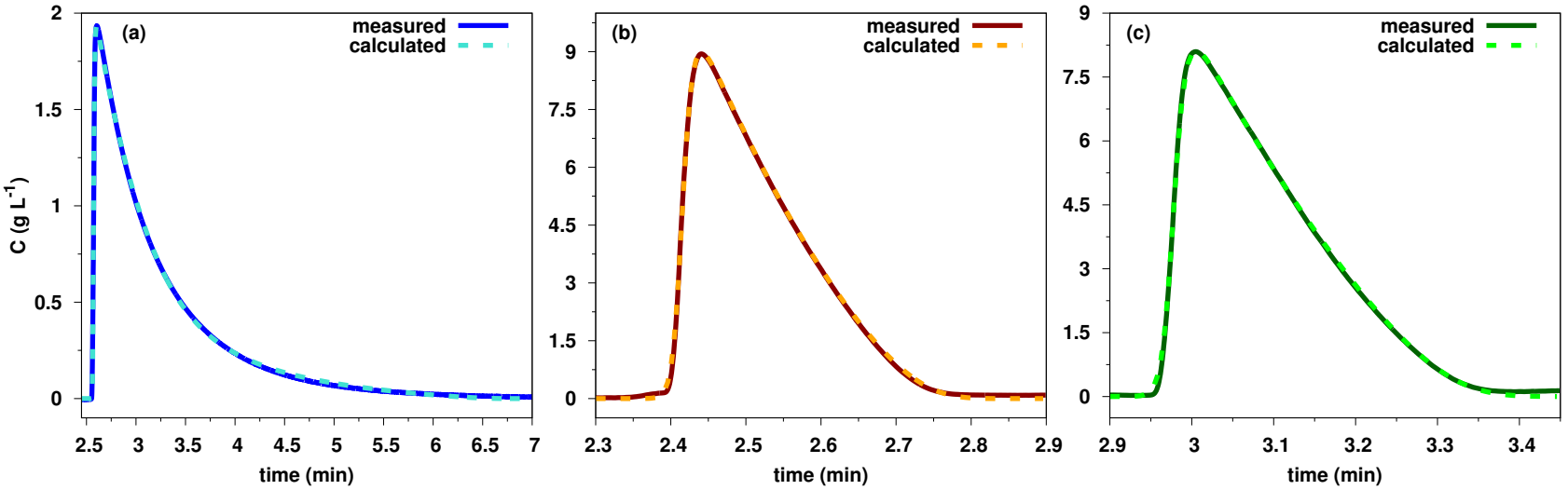

Fig. 5.4: Measured and calculated profiles obtained by the inverse method for methanol (a), octylbenzene (b) and decylbenzene (c). The agreement is very good, proving the bi-Langmuir isotherm is a suitable choice to model the adsorption energy distribution of the heterogeneous surface.

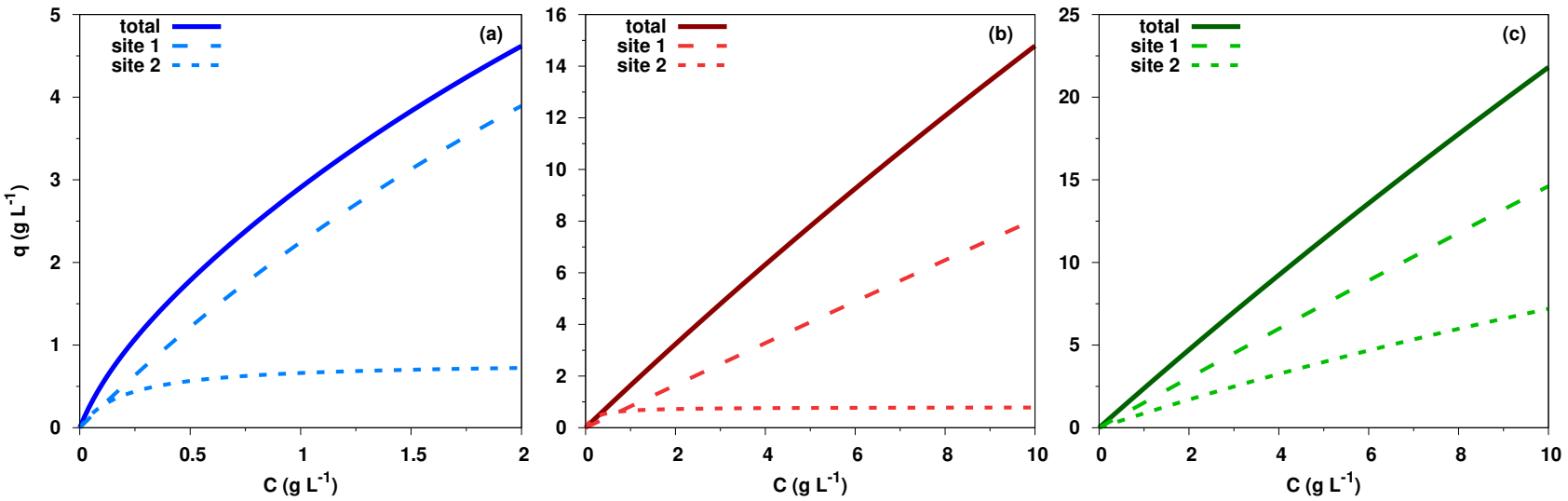

Fig. 5.5: Isotherm curves of methanol (a), octylbenzene (b) and decylbenzene (c). Note how methanol enters the nonlinear range of the isotherm while the alkylbenzenes mainly remain in the linear range due to severe dilution after the injection process. Behavior of the two different sites is also noteworthy.

5.1.3 *In silico* experiments

Competition of the individual alkylbenzenes against methanol was modeled with the competitive bi-Langmuir isotherm. The model was assembled from the previously determined single-component isotherm parameters using a similar numerical approach as previously. The constructed algorithm generated concentration versus time chromatograms. By changing the initial concentration parameters of the analyte and solvent, a wide range of cases can be investigated.

Fig. 5.6 shows how the retention and peak profiles of octylbenzene (a) and decylbenzene (b) changed with the amount of methanol. The initial alkylbenzene concentration was set to the actual concentrations of the sample injected during the preliminary studies (2.2 g/L for C_8 and 3.4 g/L for C_{10}), while the concentration of methanol was increased gradually from 0 to 792.0 g/L so the final step represented the real injections. In the actual sample, the concentrations of the analytes were negligible compared to the amount of methanol, while their adsorption was influenced by the solvent. The adsorption of methanol, however, remained unaffected by the alkylbenzenes. During the simulations, the retention time of methanol was $t_{\mathrm{MeOH}} = 6.35$ min, while for the alkylbenzenes at step 1, with no methanol present it was $t_{\mathrm{C8}} = 2.62$ min and $t_{\mathrm{C10}} = 3.19$ min.

In both cases, retention decreased as the concentration of methanol increased. In addition, band compression and in the case of decylbenzene, peak distortion could be observed. The observations can be linked to the displacement effect. Competition occurred in the nonlinear range of the isotherm resulting in methanol disturbing the adsorption of the analytes and ultimately acting as a displacing agent. In the case of decylbenzene, the competition induced overlapping bands with the solvent, producing abnormal peak shapes and apparent efficiency.

Two hypothetical solutes, H1 and H2, both set at 5.0 g/L concentration were also investigated by modifying the isotherm parameters a_1 and a_2. The retention time of H1 was set at $t_{\mathrm{H1}} = 4.15$ min meaning a stronger retention than decylbenzene but weaker than methanol, while H2 was set at $t_{\mathrm{H2}} = 8.74$ min which meant a stronger retention than methanol. The changes in retention and peak shapes of H1 (a) and H2 (b) are illustrated in Fig. 5.7.

H1 was affected by the same displacement effect but with a more severe outcome, displacement was more emphasized. H2, however, exhibited the tag-along effect caused by the abundance of the weakly adsorbing methanol, prohibiting the adsorption process of the compound by acting as an inhibitor and blocking access to the adsorption sites. This resulted in elongated bands and decreased apparent efficiency.

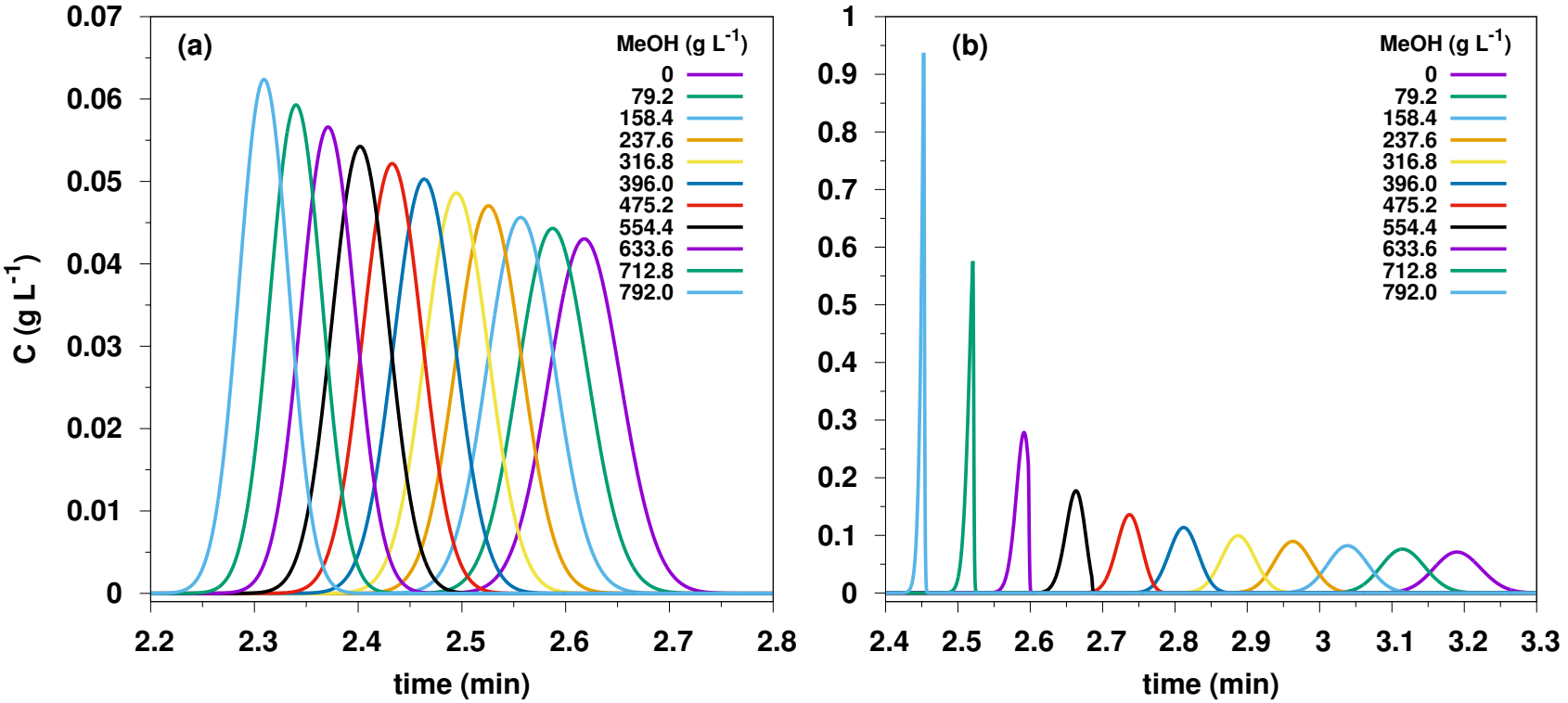

Fig. 5.6: Results of *in silico* experiments of octylbenzene (a) and decylbenzene (b). As methanol content increased, retention of the compounds decreased in both cases and the displacement effect could be observed.

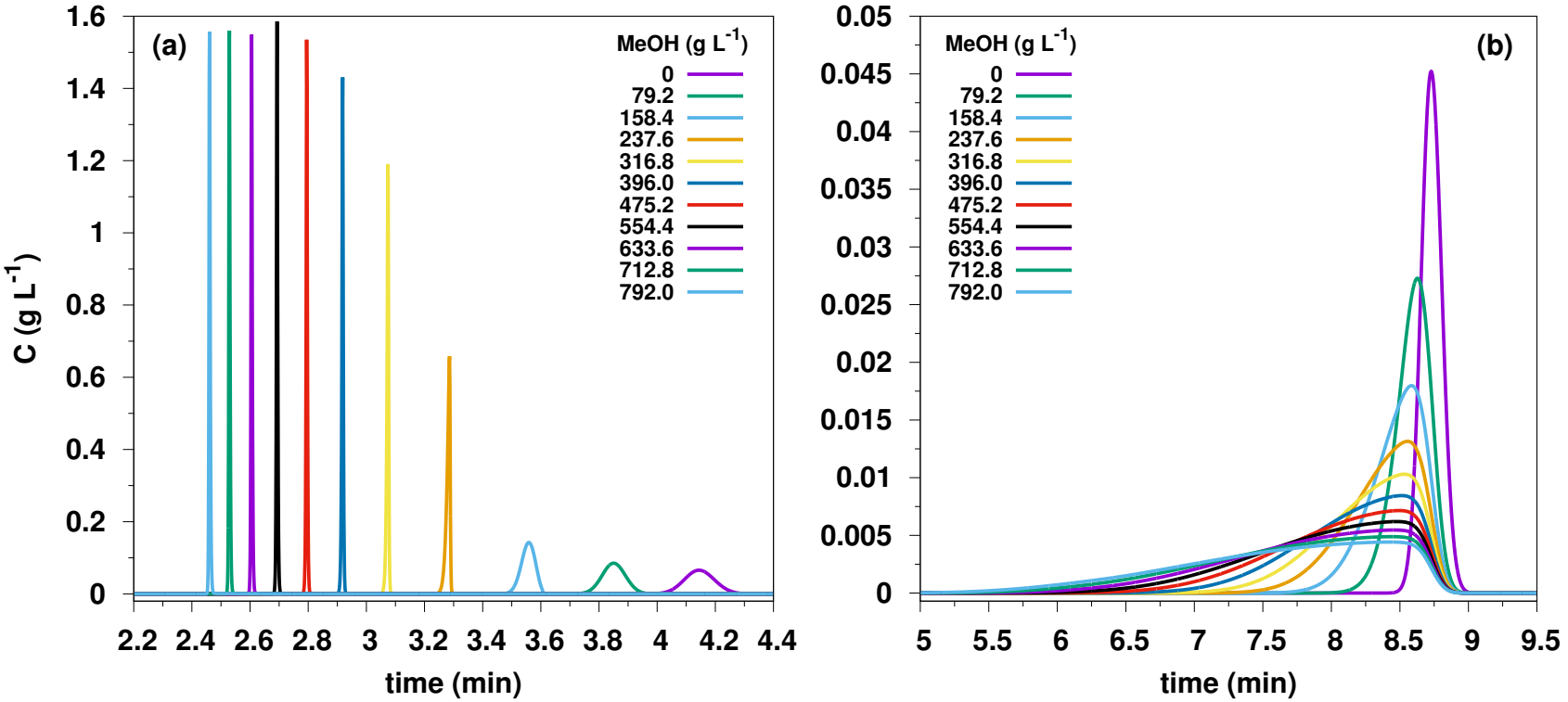

Fig. 5.7: Results of *in silico* experiments of hypothetical compounds H1 (a) and H2 (b). Retention decreased with increasing methanol content. While the displacement effect was observed in the case of H1, H2 was affected by the tag-along effect.

5.2 The influence of flow meter placement, conditions and injections on mass flow

The influence of several factors on mass flow measurements is discussed in this section. First, options for the placement of the flow meter and pressure gauge around the column are compared. Then, the effect of pressure and temperature (Table 4.3) on mass flow rate is evaluated and lastly, we investigate whether there is a significant difference between the mass flow rate at equilibrium and when it is disturbed by injections.

5.2.1 Placement of the flow meter and pressure gauge

For the mass flow rate, configurations II and III (Fig. 4.1) were compared first, representing the column inlet and outlet, respectively, from the perspective of the CFM. These two positions allow for the observation of the mass flow rate directly before and after the column. It is important to note that all mass flow rates presented here were measured at equilibrium (recorded after 30 minutes of equilibration).

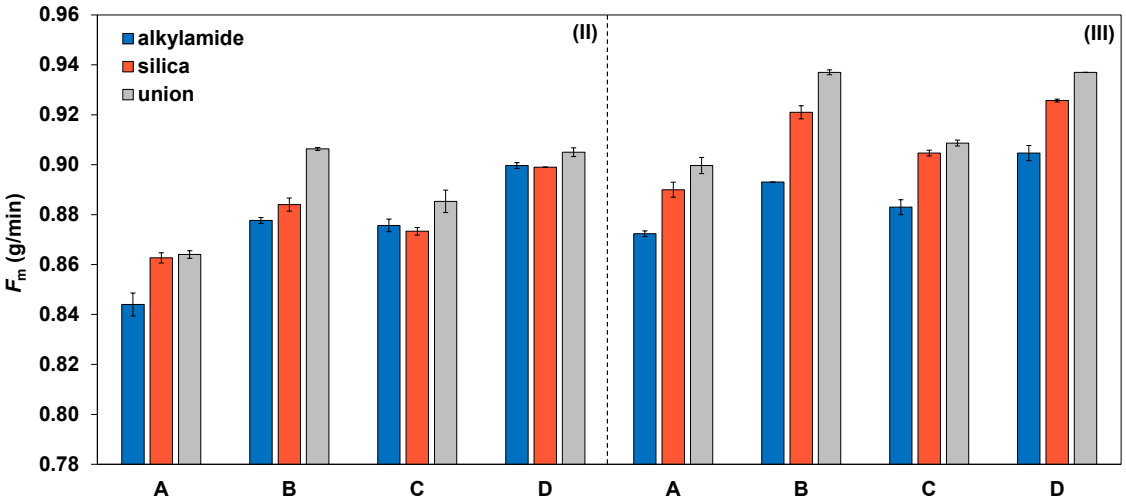

Fig. 5.8: Mass flow rates measured at the inlet (II) and the outlet (III) of the alkylamide and silica columns as well as the zero-volume union, for the four set of experimental parameters (A through D).

Figure 5.8 shows the mass flow rates for the two columns employed in this study, the ABZ+Plus alkylamide and Spherisorb Silica 5 μm columns as well as for the union. Standard deviations calculated from the replicate measurement are also indicated. The data was plotted side-by-side for a better presentation of the positions, columns and experimental conditions at the same time.

In every case, different mass flow rates were measured at the inlet and the outlet, which can be attributed to the CFM altering the configuration of the system. When the CFM is at the inlet, it introduces a slight restriction in the way of the flow at that point. At the outlet, the restriction is introduced after the mobile phase has passed through the column. However, this difference in mass flow is only apparent, since no mass is generated or lost in the system. The well-defined difference between the columns can be attributed to column length as well as particle size, with the alkylamide phase composed of 3 μm particles and the silica phase composed of 5 μm particles. Undoubtedly, mass flow rates were highest in the case of the union.

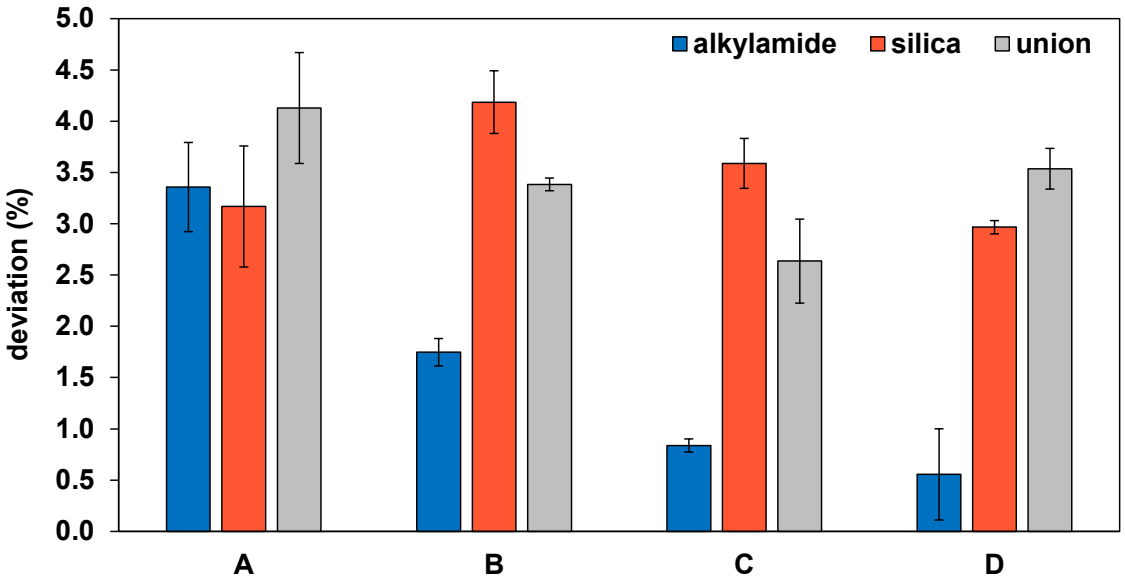

Fig. 5.9: Deviation of mass flow rates between the inlet and outlet of the columns for all experimental conditions, where the inlet was used as reference for calculations. The data shows different tendencies for different columns with significant deviations in some of the cases ranging between 0.6 and 4.2%.

The difference in mass flow rates between the inlet and outlet is plotted in Fig. 5.9 with the inlet used as reference. The two columns show different tendencies as the experimental conditions change. In the case of the alkylamide column, deviation from the inlet is highest with 3.4% (0.028 g/min) at 20 °C and 104 bar (setting A) that gradually decreases as first pressure (setting B), then temperature (setting C) is raised separately, settling at 0.6% (0.005 g/min) at 40 °C and 150 bar (setting D). The deviation was highest with 4.2% (0.037 g/min) at setting B for the silica column, while the union showed a difference of 4.1% (0.036 g/min) at setting A.

Configurations I and II, then III and IV were evaluated for same-side comparisons, representing inlet/inlet and outlet/outlet positions, respectively. Theoretically, no major differences should be expected at the same side and this was, with few exceptions, mostly true. At the inlet positions, the two columns showed decreasing tendencies going from 2.8 (0.024 g/min) to 0.1% (0.001 g/min) for the alkylamide column and 1.6 (0.014 g/min) to 0.1% (0.001 g/min) for the silica column. The union maintained a more uniform range between 1.0 (0.009 g/min) and 1.8% (0.015 g/min). The differences were less emphasized at the outlet side ranging between 0.1 (0.001 g/min) and 2.2% (0.020 g/min). Testing showed that the pressure gauge in positions I and IV had no effect on the mass flow rate and the low standard deviation values eliminate a repeatability error of the experiments, so the small differences remain a curiosity.

Regarding the pressure, configurations II and III represent the outlet and inlet, respectively, from the perspective of the pressure gauge. Measuring pressure in these positions is required for volumetric flow rate determination along with the mobile phase density. The differences provide values of pressure drop along the columns (plotted in Fig. 5.10) that are in good agreement with dimensions and particle sizes of the columns.

Configurations I and III are inlet positions that give information about pressure drop on the CFM present in position I. Fig. 5.11 shows that pressure drops were around 1.5 bar for the columns and 2 bar for the union. Looking at the outlet side (positions II and IV), pressure drops were significantly lower with values ranging

between 0.1 and 0.3 bar in all cases. The results suggest that the mass flow meter has a slight effect on mobile phase flow, especially upstream the column.

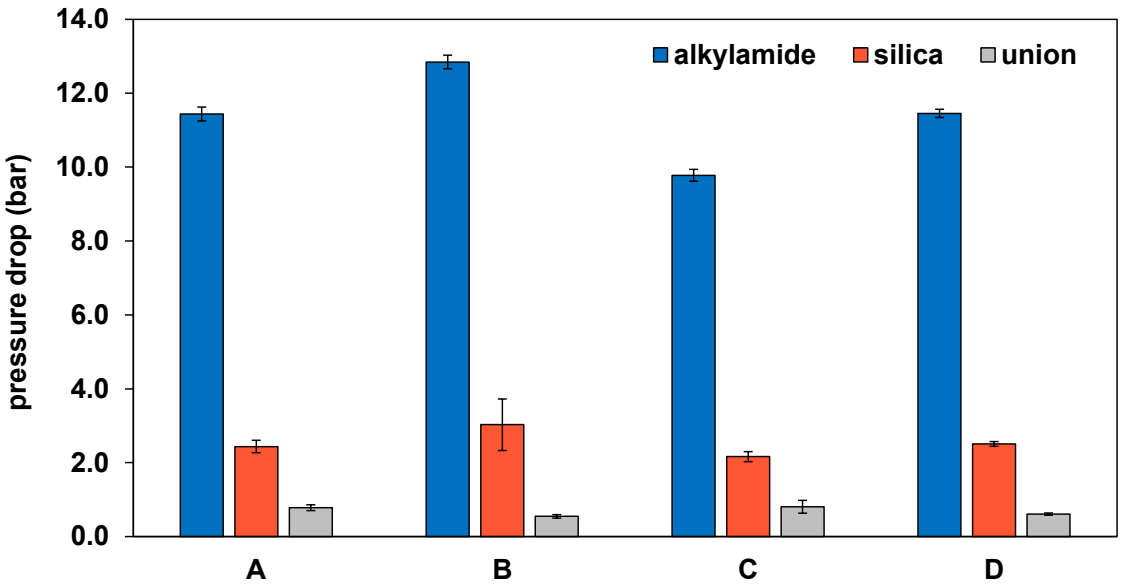

Fig. 5.10: Pressure drop values along the columns and zero-volume union for all operating conditions, calculated from the pressure gauge readings as $\Delta p = P(\mathrm{III}) - P(\mathrm{II})$. The alkylamide column showed noticeable differences due to length and particle size.

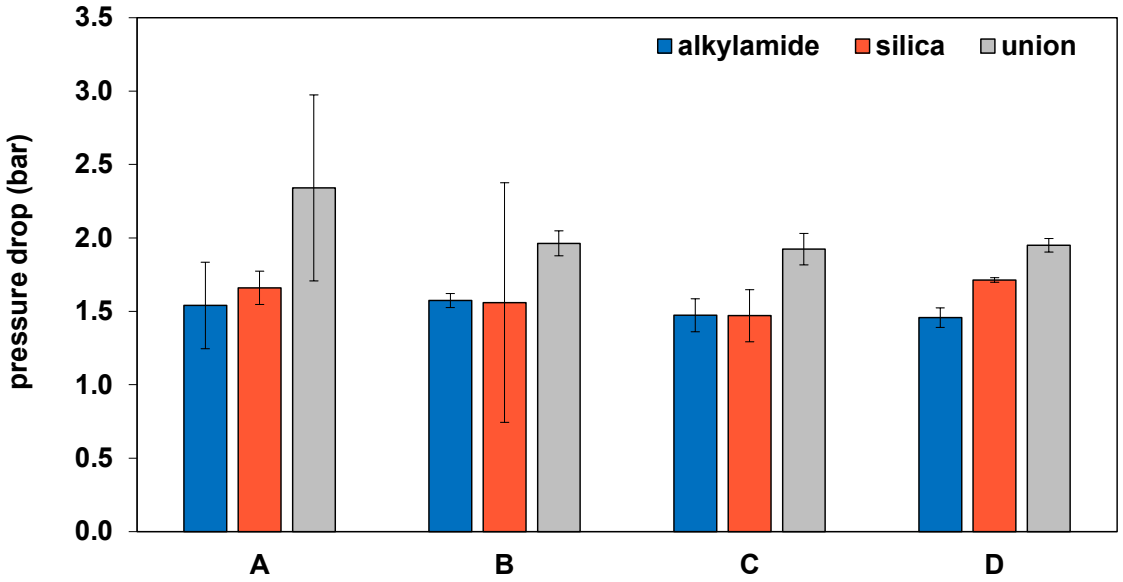

Fig. 5.11: Pressure drop values on the CFM at the inlet side for all conditions, calculated from the pressure gauge readings as $\Delta p = P(\mathrm{III}) - P(\mathrm{I})$. The results suggest a slight effect on mass flow rate upstream the column. Pressure drops at the outlet were negligible.

System pressure and pressure gauge readings are provided for the alkylamide column in Table 5.2. The readings show that when the pressure gauge is at the column inlet (configurations I and III), system pressure and pressure gauge values were close with 2% discrepancies at most. At the outlet (II and IV) however, the differences (11% at most) came from the pressure drop on the column. A similar behavior was observed for the silica column and the union showed no significant differences.

Table 5.2: System pressure (pump) and pressure gauge (P) readings in the case of the alkylamide column.

configuration	setting	pump (bar)	P (bar)
I	A	122.07	121.49
	B	169.37	169.22
	C	120.73	120.05
	D	168.00	167.84
II	A	121.37	108.51
	B	168.57	154.80
	C	121.03	108.80
	D	168.00	154.93
III	A	122.40	119.95
	B	169.50	167.65
	C	120.90	118.57
	D	168.20	166.38
IV	A	121.80	108.86
	B	169.10	154.95
	C	120.43	108.91
	D	167.57	155.05

5.2.2 The effect of pressure and temperature on mass flow rate

The influence of the back pressure regulator and column thermostat settings on mass flow rate is discussed in this section. The previous comparisons showed that the point of measurements affected the mass flow rate, however, the operating conditions also had an important role. Changes in mass flow rates due to pressure and/or temperature raise were calculated for all configurations, columns and conditions, with setting A used as base level (Fig. 5.12).

The results show similar tendencies in all positions. Raising back pressure to 150 bar (setting B) had significant effects, with mass flow rates increasing by 2.4–5.3% (0.021–0.045 g/min) both at inlet (I and II) and outlet (III and IV) positions. Raising temperature to 40 °C had minimal effect at the outlet positions (1.0–1.6% or 0.009–0.015 g/min), while the inlet showed more varied results (0.4–3.8% or 0.004–0.032 g/min). Raising both parameters together significantly increased mass flow rates with changes between 3.5 (0.030 g/min) and 6.6% (0.056 g/min), due to the higher influence of pressure on the density of the mobile phase.

5.2.3 The effect of injections on mass flow rate

In this section, we explore the difference between the mass flow rate taken at equilibrium and when it is continuously recorded while injections are made. Vajda et al. studied the effect of injections and found that the mass flow rate dropped significantly after an injection was made [65]. They proposed that the average between the injection time and retention time should be used for calculations.

Fig. 5.13 shows an example of the mass flow rate profile during an experiment (alkylamide column, position I and condition A). The first drop at 0.5 min is related to the preparation process of the autosampler. The injection happens at $t_{\mathrm{inj}} = 1.1$ min, where mass flow rate drops to 0.570 g/min, signifying a severe 34% difference in comparison to 0.867 g/min at equilibrium.

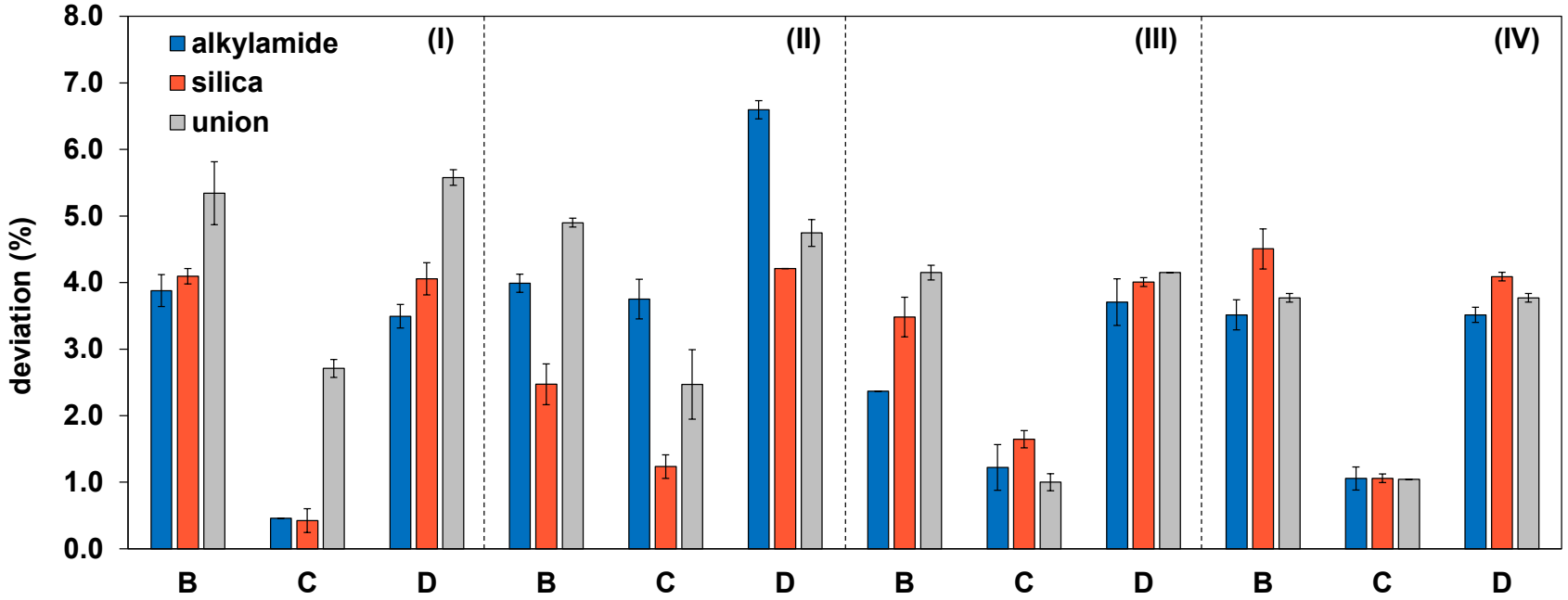

Fig. 5.12: Changes in mass flow rates for all columns, positions and conditions, with setting A (20 °C and 104 bar) used as reference. The result show significant increases in cases when pressure was raised, while temperature alone only resulted in minimal changes.

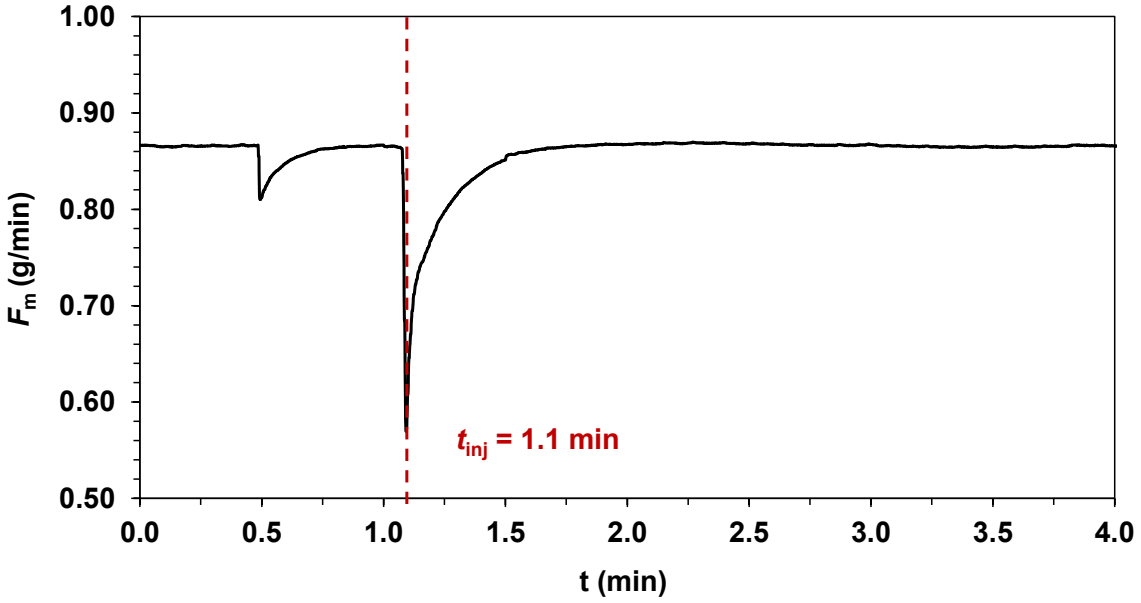

Fig. 5.13: Mass flow rate profile in the case of the alkylamide column, position I and condition A. The injection inflicts a drop to 0.570 g/min from the equilibrium value of 0.867 g/min, resulting in a 34% difference. The negative peak related to the injection translates to a mass deficit of 0.033 g if integrated until the hold-up time (1.56 min).

New mass flow rates accounting for the injection and their deviation from the equilibrium were calculated by the above mentioned method for all columns, conditions and configurations. Hold-up times were chosen as endpoints of the average calculations, but since their measurements were performed with no CFM or pressure gauge, the results only give an estimation for the different positions. Fig. 5.14 shows the differences between the equilibrium and the disturbed average mass flow rates for all conditions, positions and both columns. Undoubtedly, mass flow rates were more affected in the case of the silica column (0.7–4.2% or 0.006–0.037 g/min) than the alkylamide (0.1–2.8% or 0.001–0.025 g/min), that can be expected due to the shorter length and larger particle size of the former. In addition, deviations were relatively less pronounced at elevated pressures (settings B and D) as a result of a more compressed mobile phase that proved to be more resistant to fluctuations. Eventually, differences were significant but still remained rather low across the board.

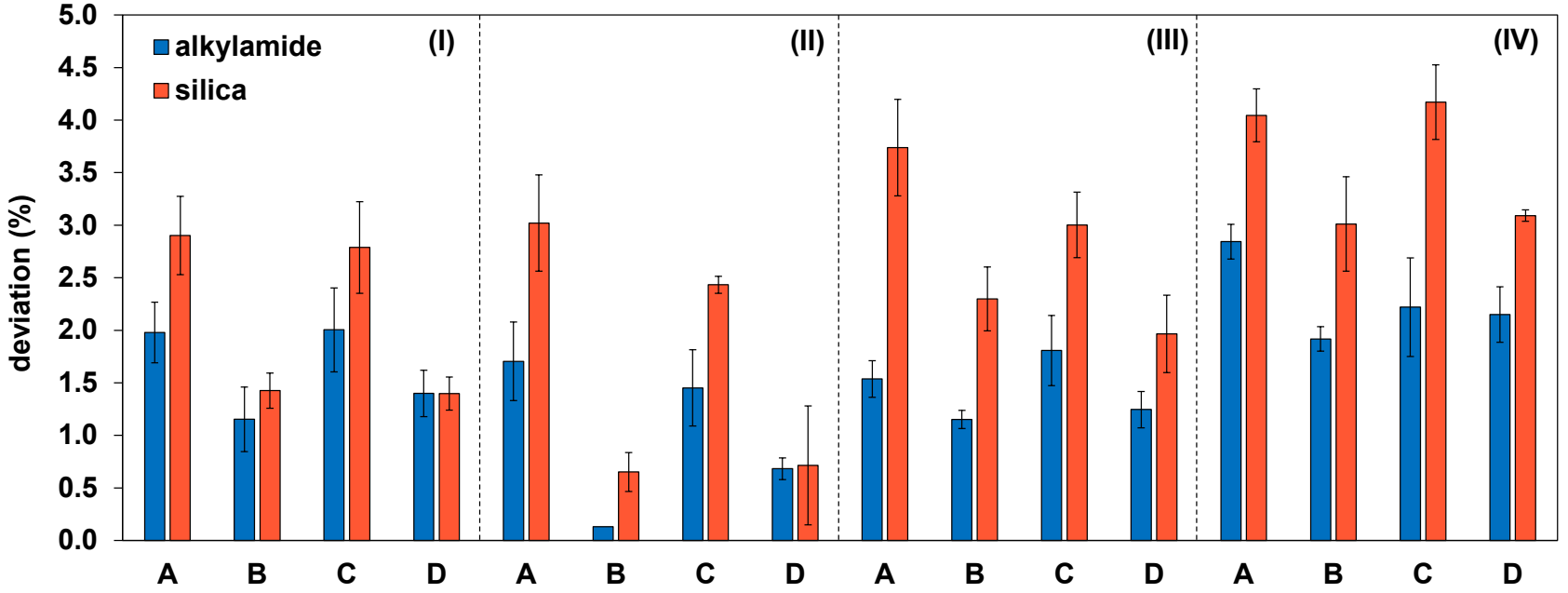

Fig. 5.14: Differences between the mass flow rates at equilibrium and when injections are accounted for. The silica column produced more pronounced deviations due to its shorter length and larger particle size while the alkylamide column often stayed around 1%. In the case of higher pressures, the mobile phase proved to be less prone to fluctuations.

5.3 Exploring the application limits of different hold-up time markers

This section focuses on our results related to the study of different hold-up time markers. The first part details sample preparation, stability studies and method development, then some initial results of possible tracer compounds are discussed. Then, a more detailed comparison is made between nitrous oxide and other markers that have been used in different fields of SFC. Next, the effect of the organic modifier, namely methanol is studied in detail. Lastly, we look into the possible effect of the stationary phase.

5.3.1 Method development

Our early studies focused on method development for proper nitrous oxide detection. For this purpose, several experiments were performed with neat methanol, hexane and nitrous oxide dissolved in methanol, all three used as possible unretained markers. The chosen default conditions were neat carbon dioxide mobile phase, 20 °C and 104 bar back pressure with the ABZ+Plus alkylamide column. The experiments were performed with and without the Coriolis flow meter connected to the system.

The results showed that nitrous oxide was the best compound out of the three since it exhibited the lowest elution time. Due to the neat carbon dioxide mobile phase, methanol was immediately adsorbed on the stationary phase and was eluted with a large diffuse band at later retention times. Hexane eluted slightly later than nitrous oxide and due to its lower purity the signal was unsuitable for evaluation. Experiments performed with and without the CFM connected to the SFC system proved that the unit should not be connected for separations due to the large volume and band broadening effect added, as shown in Section 4.3.2.

Sample preparation time of nitrous oxide was investigated as well, with 1, 2 and 5 minutes of bubbling of the gas in methanol. Injections made with the three samples showed that longer times had no beneficial effect. On the contrary,

the longer the sample preparation time, the lower the intensities, peak areas and peak widths, meaning that nitrous oxide reaches the highest concentration in methanol in one minute out of the three investigated cases (Fig. 5.15). Based on these findings, 1 minute should be sufficient for sample preparation.

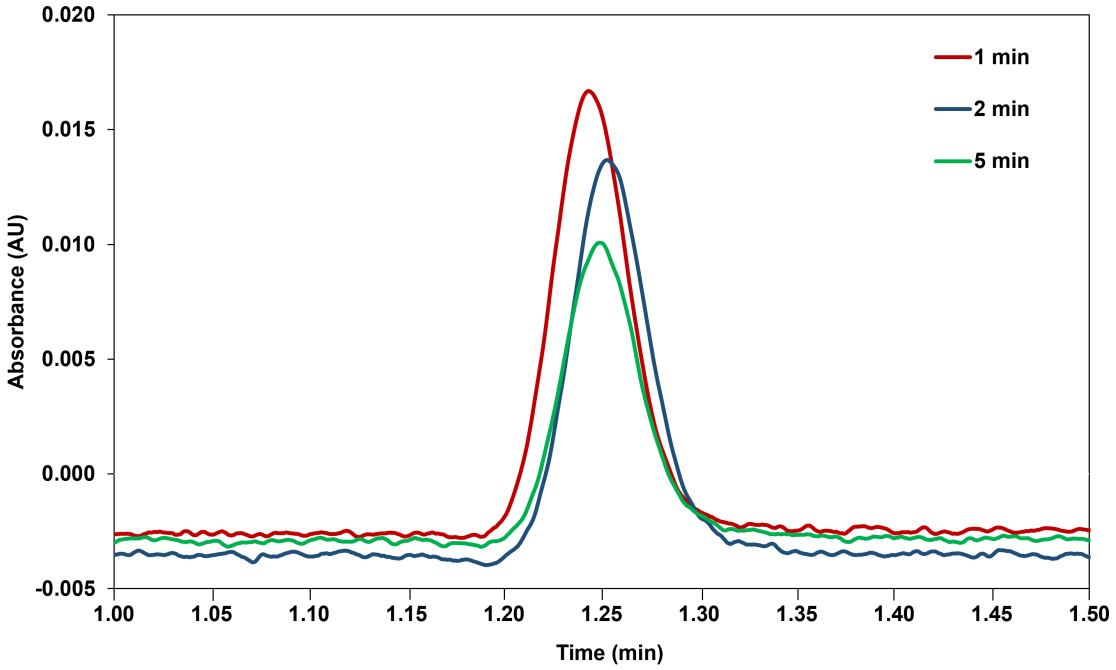

Fig. 5.15: The effect of sample preparation time on the concentration of nitrous oxide.

Stability of the nitrous oxide sample was also studied. Literature states that the sample in unstable and a fresh one should be prepared every couple of hours [59]. Our experiments approximately confirmed this statement. A fresh sample was prepared, measured immediately and then measured again at different intervals. Fig. 5.16 shows that after 9 hours, the sample still retained 67% of its initial concentration. After 24 hours, however, the intensity of the peak decreased to around one quarter of the original signal.

5.3.2 Comparison of different markers

After the preliminary studies, different compounds were compared that have been used previously as hold-up time markers in SFC, namely hexane, acetone (10 V/V% in MeOH), nitrous oxide (1 min in MeOH) and TTBB (0.01 mg/mL). Neat acetone

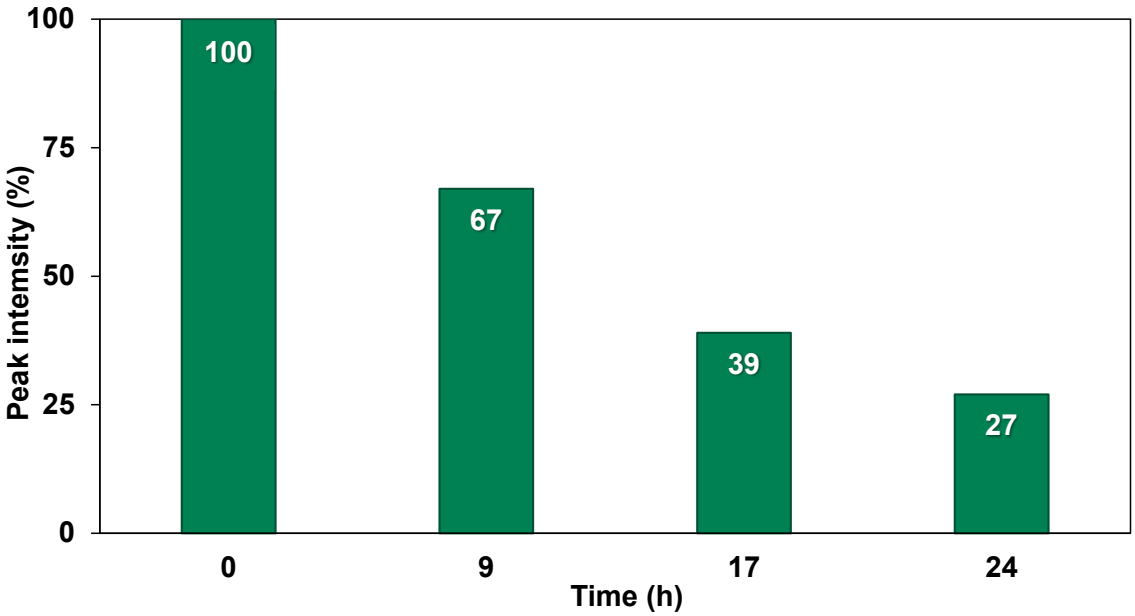

Fig. 5.16: Degradation of the nitrous oxide sample with the passage of time.

proved to be too concentrated resulting in distorted peak shapes hence the dilution in methanol. A series of experiments were performed using two of the columns, Spherisorb Silica 5 μm and ABZ+Plus alkylamide, and the four set of settings for the column thermostat and back pressure regulator detailed in Table 4.3 (Settings A through D). The mobile phase was neat carbon dioxide.

The results showed that hexane behaved in each case as expected; unreliable, noisy signal with disturbances and impurities. In the case of the silica column, the elution time was equal to that of the nitrous oxide signal, while for the alkylamide column a slight retention could be observed. Nitrous oxide exhibited optimal, well-resolved peaks for all experiments and again proved to be the best marker for hold-up time. Acetone was significantly retained in all cases. Moreover, it also overloaded both columns, detected as a large solvent band with a diffuse rear part followed immediately by the similar solvent band of methanol. TTBB was also retained in all conditions, although to a lesser extent, detected around 0.2–1 minute later than nitrous oxide. Fig. 5.17 shows the comparison of the four markers in the case of the alkylamide column, 20 °C and 104 bar (Setting A). For the sake of proportionate comparison, hexane and N_2O were plotted at 195 nm, while acetone and TTBB were plotted at 270 nm.

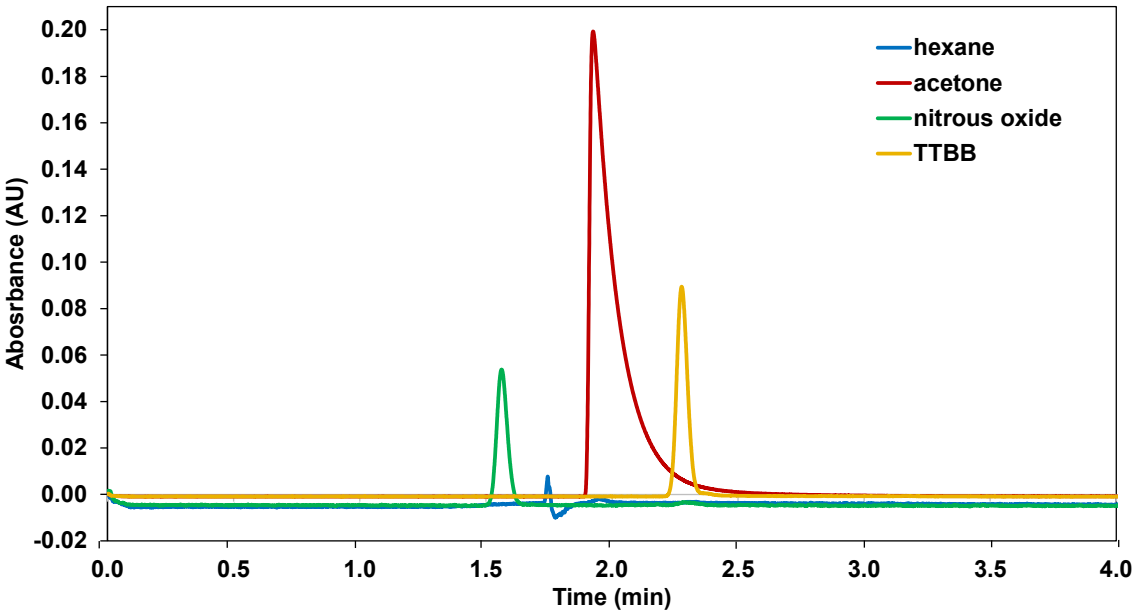

Fig. 5.17: Comparison of different hold-up time markers in the case of the alkylamide column, 20 °C and 104 bar.

5.3.3 The effect of the organic modifier

The next factor investigated was the amount of organic modifier in the mobile phase. For this purpose, a series of measurements were carried out with mobile phases containing 5, 10, 15 and 20% of methanol as organic modifier. The samples, temperature and back pressure settings were the same as in Section 5.3.2. The mobile phase compositions were tested on the Spherisorb Silica 5 column, while for the alkylamide column only 5% of methanol was used.

In the case of the silica column at 5% of methanol, nitrous oxide could be detected with a reliable peak shape and good S/N ratio, although with very little intensity in the range of 200–220 nm. The chromatogram of hexane was again scattered with disturbances and noise, however, the general elution time was very similar to the elution time of nitrous oxide with methanol present in the system. Over 210 nm, hexane gave a signal closely resembling system peaks in LC. Acetone and TTBB were still retained, although their detection was much easier due to their distinct local absorbance maxima at around 270 nm.

One of the most important hardships of N_2O measurements in SFC is the UV cutoff wavelength of most organic solvents. Unfortunately, this was the case at

10, 15 and 20% of methanol in the mobile phase, since this solvent has a cutoff wavelength of 205–210 nm and thus masked the signal of nitrous oxide, whose concentration in the sample was already very low. Acetone and TTBB could be detected, but with significant fronting. For comparison, Fig. 5.18 shows a PDA spectrum of nitrous oxide recorded at 5% of methanol, while Fig. 5.19 shows the spectrum recorded at 10%. The former shows how nitrous oxide could easily be detected at around 1.1 minutes using 5%, while the latter shows that at 10% the signal was almost nonexistent and merged into the distorted system peak caused by the sample solvent.

In the case of the alkylamide column and 5% of methanol, none of the markers provided usable signals. Hexane showed similar behavior as before, acetone and TTBB gave signals with shouldering and significant fronting, and nitrous oxide could not be detected at all, so this column was not pursued any longer.

Additional testing was performed with the (S,S) Whelk-O1 chiral stationary phase using 0–5% of methanol and our findings were very similar to those observed previously. Acetone gave a signal closer to the estimated hold-up time, although shouldering was also observed. Nitrous oxide could not be detected if any amount of methanol was present in the mobile phase.

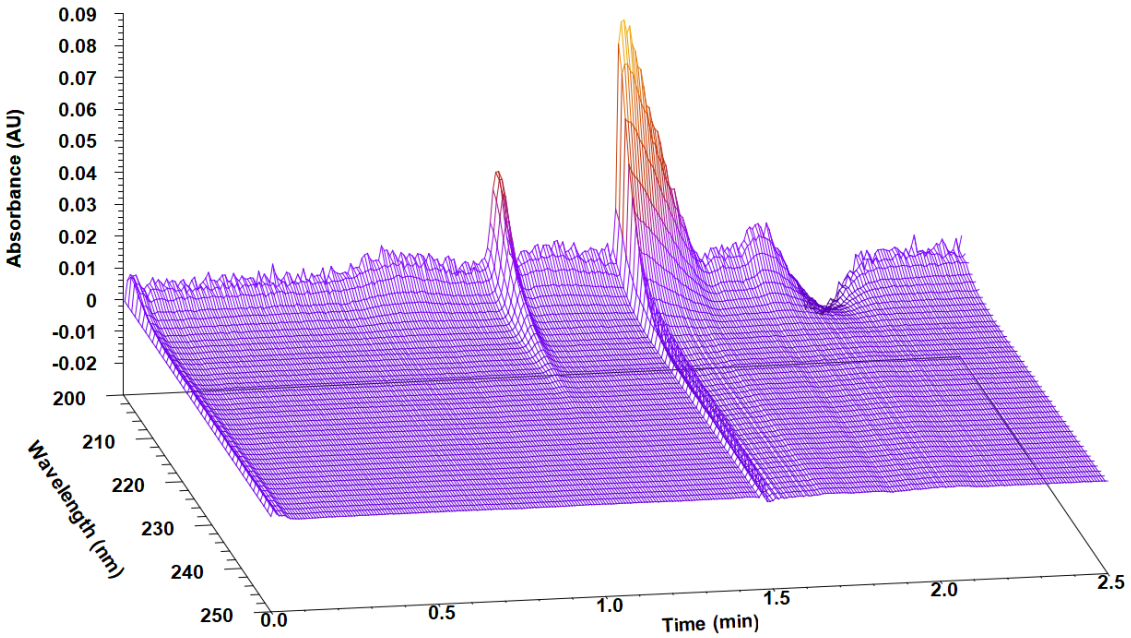

Fig. 5.18: PDA spectum of nitrous oxide at 5% of methanol on the Spherisorb 5 column.

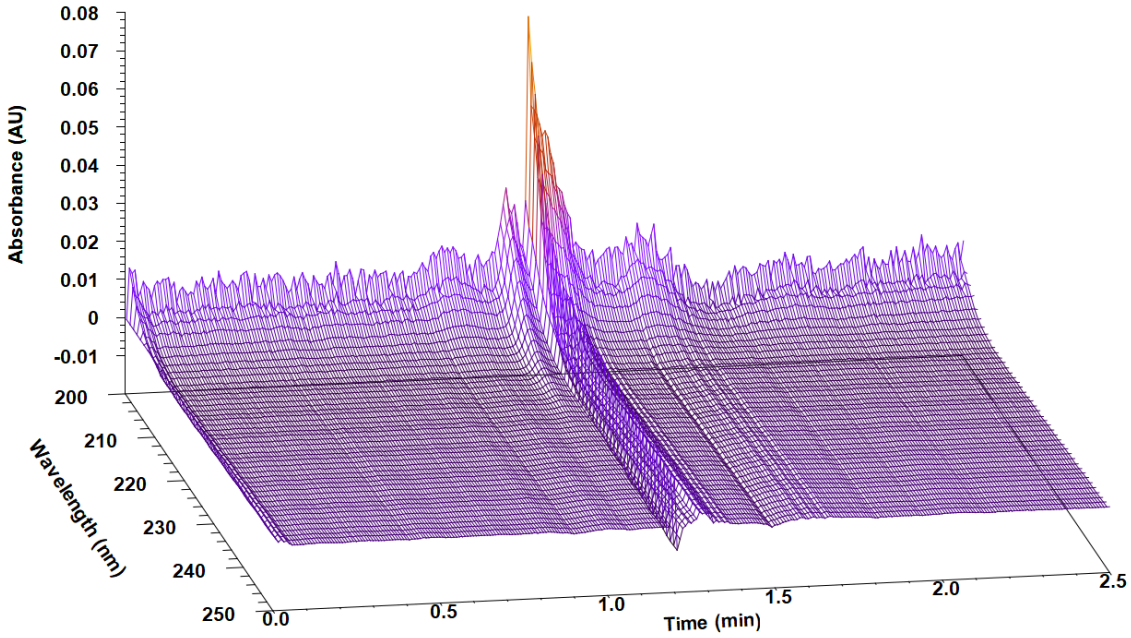

Fig. 5.19: PDA spectum of nitrous oxide at 10% of methanol on the Spherisorb 5 column.

5.3.4 The effect of the stationary phase

In theory, the stationary phase chemistry should not affect the behavior of unretained markers, especially nitrous oxide that should not exhibit any adsorption or competition on most adsorbent surfaces. In any case, a selection of stationary phases (Section 4.3.3) were tested with the exception of the previously studied columns (Spherisorb 5, ABZ+Plus and (S,S) Whelk-O1). The samples were once again the same as detailed in Section 5.3.2. The mobile phase contained 5% of methanol as organic modifier.

On the Symmetry C_{18}, acetone was slightly retained and gave a signal just after the system peak. TTBB had significant retention, as anticipated, and nitrous oxide could not be detected unfortunately. Spherisorb 10 behaved very similarly to Spherisorb 5 since the only difference in the columns was the particle size. Nitrous oxide could be detected, although barely, while acetone and TTBB were retained.

Nitrous oxide was a suitable marker for Viridis BEH and Torus DIOL, while the other samples gave unreliable and unclear signals. Fig. 5.20 shows a comparison of nitrous oxide chromatograms on the different stationary phases. The black arrows mark the peaks of nitrous oxide in each case. The different elution times (1.169 min for Spherisorb 10, 0.638 min for Viridis BEH and 0.590 min for Torus DIOL) are due to the different column dimensions.

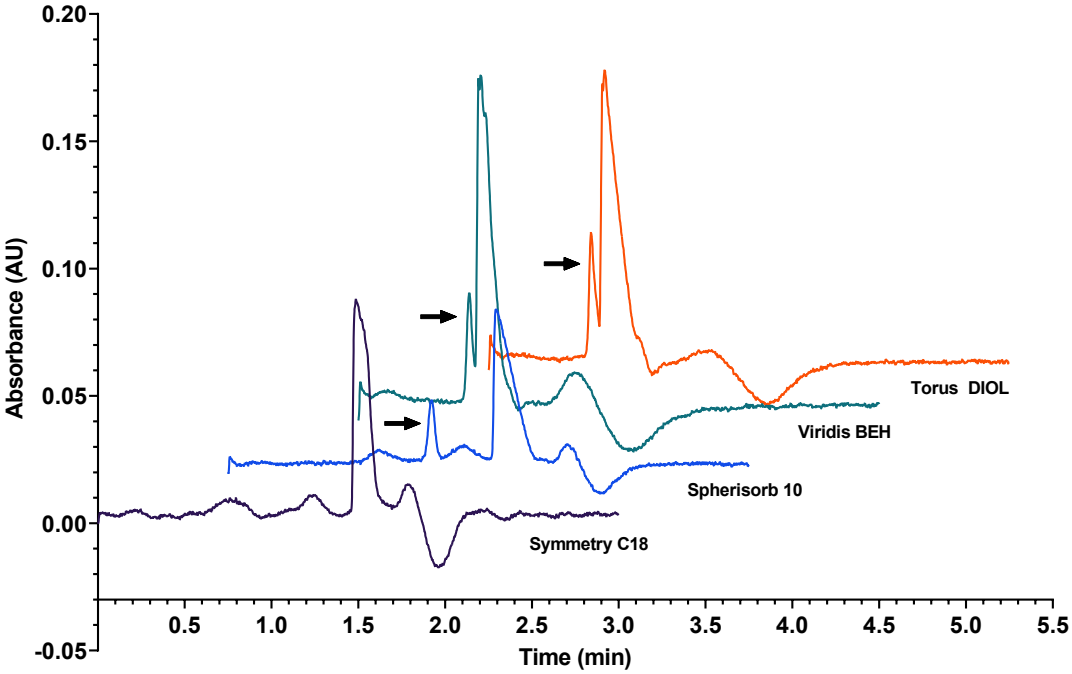

Fig. 5.20: Detection of nitrous oxide on various columns at 5% of methanol and 200 nm.

6

Conclusion

The competitive adsorption of the sample solvent and solutes was investigated in supercritical fluid chromatography. A series of n-alkylbenzene homologues were chosen as model compounds along with acetonitrile, methanol and heptane as sample solvents. After a series of preliminary experiments, the phenomenon was successfully detected with an alkylamide column, at 60 °C temperature, 150 bar back pressure and neat carbon dioxide mobile phase. In the case of methanol, the competition was easily identified based on the decreased column efficiency, shifts in retention times and changes in peak widths, since the variation of these properties was highest around the methanol band.

Single-component isotherm were determined for methanol and two alkylbenzenes surrounding the solvent band. To account for the adsorption energy distribution of the heterogeneous surface of the stationary phase, the bi-Langmuir isotherm was selected and the parameters were determined by the inverse method using a numerical method where the differential mass balance equation given by the equilibrium-dispersive model was integrated by a modified Rouchon algorithm. The results showed a very good agreement between the experimental and calculated band profiles and the behavior of the two different adsorption sites were also explored, all compounds favored site 1 by around two orders of magnitude in terms of the saturation capacity.

The competitive bi-Langmuir isotherm was chosen to model the competition. The model employed the determined parameters and a similar numerical approach as before. A series of *in silico* experiments were performed where all solute concentrations were set in the analytical range and the amount of the solvent was increased step by step to imitate the real injections. Besides the alkylbenzenes, two hypothetical solutes (H1 and H2) were also investigated with varying retentions

compared to methanol. Octylbenzene, decylbenzene and compound H1 were all affected by the displacement effect caused by the strongly adsorbing methanol acting as a displacing agent, resulting in distorted, compressed band profiles and anomalous efficiency. Compound H2 was affected by the tag-along effect caused by the abundance of methanol acting as an inhibitor, resulting in elongated peak shapes and decreased efficiency.

Our work regarding the behavior of mass flow demonstrated that even though mass flow rate is the only flow parameter considered constant in SFC, some variation can be still expected when taken at different parts of the chromatographic instrument, since the CFM alters the system configuration. Comparing mass flow rates between the inlet and outlet of the columns showed diverse tendencies in differences ranging from 0.6% to 4.2%. Considering that only neat CO_2 was used as mobile phase in the study, deviations were not too severe. In the case of mobile phases containing organic modifier and additives as well, even lower differences should be expected. Additional precision studies revealed that measuring accurate, reproducible mass flow rates in a low-flow, low-viscosity environment is problematic in a standard laboratory setup even if the built-in self-diagnostics of the SFC system show no leaks, the CFM calibration is correct and all instructions are strictly followed.

Pressure measurements complementing the work showed varied pressure drops on the columns depending on their length and particle size. Interestingly, significant pressure drops were found on the mass flow meter, more pronounced at the inlet side (1.5–2 bar), that suggest a slight effect on mobile phase flow.

Studying the effect of pressure and temperature on mass flow rate showed that the former had a larger influence while changing temperature only had minimal effects. Accounting for injections showed that although the initial drop in mass flow is severe compared to the equilibrium, taking the average from the injection time until the hold-up time reduced this effect significantly. The use of well-retained compounds should further minimize the adverse effect of injections.

In terms of hold-up time markers, nitrous oxide can be a good option for supercritical fluid chromatography. It has good solubility in alcohols, sample

preparation is simple and the sample is stable enough for a day. In addition, the properties of the gas guarantee that no adsorption or competition should take place on the stationary phase during an SFC run. The preliminary studies showed that out of all tested markers, nitrous oxide demonstrated the lowest elution times, suggesting that it was unretained, while the other probes showed some amount of retention or distorted, noisy peak shapes.

However, detection was problematic, because the signal of nitrous oxide had very low intensity due to the low concentration in the sample. Its UV spectrum is also unfortunate, because the compound can be detected only in the range of 190–220 nm, where most of the organic modifiers employed in SFC have their cutoff wavelengths. Thus, the signal is masked as seen on many occasions during our experiments, especially if the mobile phase contains 10% of methanol or more.

The comparison of different columns implied that the stationary phase did have a slight effect on the detection of nitrous oxide, however, this would contradict the theory behind the use of the compound as unretained marker. With a more comprehensive study, the limit of application could be further extended.

7

Thesis points

1. I found the sample solvent methanol competing for adsorption with n-alkylbenzene homologues in the case of neat carbon dioxide mobile phases in supercritical fluid chromatography. I identified the region where competition occurred marked by decreased column efficiencies, shifts in retention times and changes in peak widths, all induced by the displacement and tag-along effects.

2. I determined the single-component adsorption isotherms of methanol and two alkylbenzenes closest to the competing methanol band using the inverse method. I confirmed the bi-Langmuirian behavior of the compounds and then constructed a numerical method using the competitive bi-Langmuir isotherm. I modeled the competition of the real and hypothetical solutes with the solvent, and proved that the sources behind the anomalous retention behavior were the displacement and tag-along effects.

3. I have shown that accurate and precise mass flow measurements in a low-flow, low-viscosity environment are problematic when recorded at different parts of the chromatographic instrument, since the flow meter alters the system configuration. The discrepancies were as high as 4.2%, although using organic modifiers in the mobile phase mitigates the severity of the differences. I have shown that the flow meter affects the mobile phase flow and adds significant extra-column volume and variance to the system.

4. I have demonstrated that pressure had a larger effect on mass flow rate than temperature did. I have also shown that injections introduce a severe drop to the equilibrium mass flow rate, but successfully reduced this adverse effect by using the averages taken from the injection time until the elution times of the compounds instead.

5. I have concluded that nitrous oxide is the best unretained marker for accurate hold-up time measurements out of the four potential markers, since this compound gave the lowest elution times. However, detection was difficult in mobile phases containing 10% or more of organic modifier, because most solvents mask the signal of nitrous oxide. Interestingly, the comparison of multiple columns showed that the stationary phase also had a slight effect on detection.

List of acronyms and symbols

BPR	back pressure regulator
CFM	Coriolis flow meter
DAD	diode array detector
DGC	dense gas chromatography
ECP	elution by characteristic point
ED	equilibrium-dispersive model
EFLC	enhanced-fluidity liquid chromatography
EMG	exponentially modified Gaussian function
FA	frontal analysis
FACP	frontal analysis by characteristic point
FID	flame ionization detector
GC	gas chromatography
HPGC	high-pressure gas chromatography
HPLC	high performance liquid chromatography
IM	inverse method
IP-RPLC	ion-pair reversed phase liquid chromatography
ISEC	inverse size-exclusion chromatography
LC	liquid chromatography
MS	mass spectrometry
NIST	National Institute of Standards and Technology
PAH	polycyclic aromatic hydrocarbon
PDA	photodiode array
PM	perturbation method
RTM	retention time method
SFC	supercritical fluid chromatography

TFA	trifluoroacetic acid
TTBB	1,3,5-tri-*tert*-butylbenzene
UHPSFC	ultra-high performance supercritical fluid chromatography

$A(t)$	absorbance at a given time
a_1	initial slope of the bi-Langmuir isotherm at site 1
a_2	initial slope of the bi-Langmuir isotherm at site 2
A_T	peak area
b_1	equilibrium constant of the bi-Langmuir isotherm at site 1
b_2	equilibrium constant of the bi-Langmuir isotherm at site 2
C_A	concentration of component A in the mobile phase
C_B	concentration of component B in the mobile phase
C_i	concentration of component i in the mobile phase
C_i^meas	measured concentration at point i
C_i^sim	calculated concentration at point i
D_a	apparent dispersion coefficient
F	phase ratio
$F_\mathrm{m,meas}$	measured mass flow rate
$F_\mathrm{v,25řC}$	volumetric flow rate at room temperature
$F_\mathrm{v,32°C}$	volumetric flow rate at 32°C
$\bar{F}_\mathrm{v}$	mean volumetric flow rate
$F_\mathrm{v,in}$	volumetric flow rate at the column inlet
$F_\mathrm{v,out}$	volumetric flow rate at the column outlet
$F_{\mathrm{v},\rho\mathrm{CFM}}$	volumetric flow rate at CFM densities
$F_\mathrm{v,set}$	set volumetric flow rate
H	plate height
$\bar{m}$	mean mass
$m_\mathrm{exp,25°C}$	expected mass at room temperate
m_inj	mass of injected sample
N	number of theoretical plates or plate count
p	pressure

$q(C)$	concentration in the stationary phase in equilibrium with the mobile phase
q_i	concentration of component i in the stationary phase
$q_{\mathrm{s},1}$	saturation capacity of site 1
$q_{\mathrm{s},2}$	saturation capacity of site 2
r_i	difference between the calculated and measured concentrations
T	temperature
t	time
t_{p}	injection time
t_{R}	retention time
u	linear velocity of the mobile phase
$\bar{V}$	average volume
V_0	hold-up or void volume of the column
V_{a}	volume of the adsorbent
V_{R}	retention volume
V_{tot}	total (geometric) volume of the column
z	distance along the column
ε_{t}	total porosity of the column
κ	sensitivity factor
μ_1	first absolute moment of the peak
μ_2'	second central moment of the peak
$\bar{\rho}$	average density
σ	standard deviation
τ	time constant of the EMG function

Publications

Publications related to the thesis

1. **Rédei, Cs.**, Felinger, A. Modeling the competitive adsorption of sample solvent and solute in supercritical fluid chromatography, *J. Chromatogr. A*, **2019**, *1603*, 348–354. **IF: 4.049**

2. **Rédei, Cs.**, Felinger, A. The impact of placement, experimental conditions, and injections on mass flow measurements in supercritical fluid chromatography, *J. Chromatogr. A*, **2022**, *1668*, 462919 **IF: 4.1**

3. **Rédei, Cs.**, Buratti, A., Catani, M., Felinger, A. Exploring the limits of application of nitrous oxide as a hold-up time marker in supercritical fluid chromatography, *Anal. Bioanal. Chem.*, under review **IF: 4.3**

Posters and presentations related to the thesis

1. **Rédei, Cs.**, Felinger, A. Investigation of the retention behaviour of alkylbenzenes on a C18 stationary phase in supercritical fluid chromatography, 11th Balaton Symposium on High-Performance Separation Methods, September 6–8, 2017, Siófok, Hungary

2. **Rédei, Cs.**, Felinger, A. Studying the competitive adsorption of alkylbenzenes and methanol in supercritical fluid chromatography, Applications of Supercritical Fluids 2018, May 17, 2018, Budapest, Hungary

3. **Rédei, Cs.**, Felinger, A. Competitive adsorption in supercritical fluid chromatography: A model, 32nd International Symposium on Chromatography (ISC 2018), September 23–27, 2018, Cannes-Mandelieu, France

4. **Rédei, Cs.**, Felinger, A. Competitive adsorption of sample solvent and analyte in supercritical fluid chromatography, 24th International Symposium on Analytical and Environmental Problems, October 8–9, 2018, Szeged, Hungary

5. **Rédei, Cs.**, Felinger, A. A minta és a minta oldószerének kompetitív adszorpciója szuperkritikusfluidum-kromatográfiában, Elválasztástudományi Vándorgyűlés 2018, November 8–10, 2018, Tapolca, Hungary

6. **Rédei, Cs.**, Felinger, A. Modeling the solute-solvent competition in supercritical fluid chromatography, 8th Interdisciplinary Doctoral Conference (IDK 2019), May 24–25, 2019, Pécs, Hungary

7. **Rédei, Cs.**, Felinger, A. Exploring the limits of nitrous oxide as a tracer in supercritical fluid chromatography, 48th International Symposium on High-Performance Liquid Phase Separations and Related Techniques (HPLC 2019), June 16–20, 2019, Milan, Italy

8. **Rédei, Cs.**, Felinger, A. Comparison of nitrous oxide and other hold-up time markers in supercritical fluid chromatography, 12th Balaton Symposium on High-Performance Separation Methods, September 11–13, 2019, Siófok, Hungary

9. **Rédei, Cs.**, Felinger, A. A tömegárammérés rejtélyei szuperkritikusfluidum-kromatográfiában, METT25, October 18–20, 2021, Egerszalók, Hungary

10. **Rédei, Cs.**, Felinger, A. Exploring the difficulties of mass fow measurements in supercritical fluid chromatography, 33rd International Symposium on Chromatography (ISC 2022), September 18–22, 2022, Budapest, Hungary

11. **Rédei, Cs.**, Felinger, A. Exploring the difficulties of neat carbon dioxide as the mobile phase in supercritical fluid chromatography, 33rd International Symposium on Chromatography (ISC 2022), September 18–22, 2022, Budapest, Hungary

Publications not related to the thesis

1. Simon, J., **Rédei, Cs.**, Felinger, A. The use of alteration analysis in supercritical fluid chromatography to monitor changes in a series of chromatograms, *J. Chromatogr. A*, **2019**, *1596*, 217–225. **IF: 4.049**

2. Kazmouz, M. Y., **Rédei, Cs.**, Felinger, A. The adsorption of methanol on reversed phase stationary phases in supercritical fluid chromatography, *J. Chromatogr. A*, **2021**, *1653*, 462386 **IF: 4.601**

Posters and presentations not related to the thesis

1. Kazmouz, M. Y.*, László, Sz.*, **Rédei, Cs.**, Bacskay, I., Felinger, A. Surface excess isotherms of organic modifier and carbon dioxide mixture in sub- or supercritical fluid chromatography, Applications of Supercritical Fluids 2018, May 17, 2018, Budapest, Hungary

2. Horváth, É., **Rédei, Cs.**, Boros, B., Felinger, A. Investigation of interactions on chiral zwitterionic stationary phases in enantiomer separation using HPLC and SFC methods, 24th International Symposium on Analytical and Environmental Problems, October 8–9, 2018, Szeged, Hungary

3. Horváth, É., **Rédei, Cs.**, Boros, B., Felinger, A. Királis vegyületek elválasztása során kialakuló kölcsönhatások elméleti hátterének vizsgálata HPLC és SFC módszerek alkalmazásával, XXIV. Nemzetközi Vegyészkonferencia, October 24–27, 2018, Szovátafürdő, Romania

4. Simon, J., **Rédei, Cs.**, Zelenyánszki, D., Felinger, A. Komplex mintakeverékből származó komponensek eredetének meghatározás és vizsgálata alterációs analízissel, Elválasztástudományi Vándorgyűlés 2018, November 8–10, 2018, Tapolca, Hungary

5. Horváth, É., **Rédei, Cs.**, Boros, B., Felinger, A. Királis kromatográfiás mérési módszerek összevetése az elválasztás során kialakuló kölcsönhatások vizsgálata alapján, Elválasztástudományi Vándorgyűlés 2018, November 8–10, 2018, Tapolca, Hungary

6. Kazmouz, M. Y., **Rédei, Cs.**, Felinger, A. Study of methanol influence on reversed phases in supercritical fluid chromatography, Elválasztástudományi Vándorgyűlés 2018, November 8–10, 2018, Tapolca, Hungary

7. Simon, J., **Rédei, Cs.**, Zelenyánszki, D., Felinger, A. Two-dimensional correlation and alteration analysis in chromatography for identifying the changes in high-dimensional data, 48th International Symposium on High-Performance Liquid Phase Separations and Related Techniques (HPLC 2019), June 16–20, 2019, Milan, Italy

8. Simon, J., **Rédei, Cs.**, Zelenyánszki, D., Felinger, A. Exploring two- and three-dimensional chromatographic data with alteration analysis, 12th Balaton Symposium on High-Performance Separation Methods, September 11–13, 2019, Siófok, Hungary

9. Kulágin, R., **Rédei, Cs.**, Lindner, W., Felinger, A. Kinidin alapú királis, ikerionos típusú állófázis öregedésének vizsgálata SFC alkalmazásával, METT25, October 18–20, 2021, Egerszalók, Hungary

Acknowledgement

I would like to express my deepest gratitude to my supervisor, Dr. Attila Felinger for his continued guidance, support and patience, and for providing me the opportunity to pursue a PhD in this field.

I would like to thank Dr. Ferenc Kilár, former head of the Doctoral School of Chemistry for all his help and support during the PhD program.

I am very grateful to Dr. Krisztián Horváth, my former supervisor at the University of Pannonia, who steered me towards the path of SFC.

I also would like to dedicate the thesis to the memory of Dr. Péter Vajda, who taught me as much as he could during our short time working together.

Many thanks to my colleagues at the Department of Analytical and Environmental Chemistry for all the help and good advice.

Last but not least, I would like to thank my friends and my family: my mom, my sister and my brother for their love, support and encouragement.

Köszönetnyilvánítás

Szeretném köszönetemet kifejezni témavezetőmnek, Dr. Felinger Attila tanszékvezető egyetemi tanárnak az útmutatásért, támogatásért, türelméért és hogy lehetőséget adott, hogy a tanszéken kezdhessem el kutatómunkámat.

Köszönönettel tartozom Dr. Kilár Ferencnek, a Kémia Doktori Iskola korábbi vezetőjének a sok segítséget és támogatást, amelyet a doktori képzés során nyújtott.

Hálás vagyok korábbi témavezetőmnek, Dr. Horváth Krisztiánnak, amiért elindított az SFC felé vezető úton.

Szeretném a disszertációt Dr. Vajda Péter emlékének ajánlani, akitől rengeteg tanultam a rövid idő alatt, amely rendelkezésünkre állt.

Köszönöm kollégáimnak az Analitikai és Környezeti Kémia Tanszéken a rengeteg segítséget és jó tanácsokat.

Végül pedig szeretném megköszönni barátaimnak és a családomnak: anyukámnak, a húgomnak és bátyámnak a szerető támogatást és bátorítást, hogy ez a munka elkészülhessen.

Bibliography

(1) Tomai, P.; Bosco, C. D.; D'Orazio, G., et al. Supercritical fluid chromatography for vitamin and carotenoid analysis: An update covering 2011–2021. *J. Chromatogr. Open* **2022**, *2*, 100027.

(2) Guiochon, G.; Tarafder, A. Fundamental challenges and opportunities for preparative supercritical fluid chromatography. *J. Chromatogr. A* **2011**, *1218*, 1037–1114.

(3) Rajendran, A. Design of preparative-supercritical fluid chromatography. *J. Chromatogr. A* **2012**, *1250*, 227–249.

(4) Miller, L. Preparative enantioseparations using supercritical fluid chromatography. *J. Chromatogr. A* **2012**, *1250*, 250–255.

(5) Berger, C.; Perrut, M. Preparative supercritical fluid chromatography. *J. Chromatogr. A* **1990**, *505*, 37–43.

(6) Pauk, V.; Lemr, K. Forensic applications of supercritical fluid chromatography-mass spectrometry. *J. Chromatogr. B* **2018**, *1086*, 184–196.

(7) Desfontaine, V.; Guillarme, D.; Francotte, E.; Nováková, L. Supercritical fluid chromatography in pharmaceutical analysis. *J. Pharm. Biomed. Anal.* **2015**, *113*, 56–71.

(8) Bernal, J. L.; Martín, M. T.; Toribio, L. Supercritical fluid chromatography in food analysis. *J. Chromatogr. A* **2013**, *1313*, 24–36.

(9) Berger, T. A. Effect of density on kinetic performance in supercritical fluid chromatography with methanol modified carbon dioxide. *J. Chromatogr. A* **2018**, *1564*, 188–198.

(10) Desfontaine, V.; Tarafder, A.; Hill, J., et al. A systematic investigation of sample diluents in modern supercritical fluid chromatography. *J. Chromatogr. A* **2017**, *1511*, 122–131.

(11) Glenne, E.; Leek, H.; Klarqvist, M.; Samuelsson, J.; Fornstedt, T. Systematic investigations of peak deformations due to co-solvent adsorption in preparative supercritical fluid chromatography. *J. Chromatogr. A* **2017**, *1496*, 141–149.

(12) Glenne, E.; Öhlén, K.; Leek, H., et al. A closer study of methanol adsorption and its impact on solute retentions in supercritical fluid chromatography. *J. Chromatogr. A* **2016**, *1442*, 129–139.

(13) Tarafder, A. Metamorphosis of supercritical fluid chromatography to SFC: An Overview. *TrAC Trends Anal. Chem.* **2016**, *81*, 3–10.

(14) De Pauw, R.; Shoykhet (Choikhet), K.; Desmet, G.; Broeckhoven, K. Effect of reference conditions on flow rate, modifier fraction and retention in supercritical fluid chromatography. *J. Chromatogr. A* **2016**, *1459*, 129–135.

(15) Klesper, E; Corwin, A. H.; Turner, D. A. High pressure gas chromatography above critical temperatures. *J. Org. Chem.* **1962**, *27*, 700–701.

(16) Saito, M. History of supercritical fluid chromatography: Instrumental development. *J. Biosci. Bioeng.* **2013**, *115*, 590–599.

(17) Karayannis, N. M.; Corwin, A. H.; Baker, E. W.; Klesper, E.; Walter, J. A. Apparatus and materials for hyperpressure gas chromatography of nonvolatile compounds. *Anal. Chem.* **1968**, *40*, 1736–1739.

(18) Jentoft, R. E.; Gouw, T. H. Pressure-programmed supercritical fluid chromatography of wide molecular weight range mixtures. *J. Chromatogr. Sci.* **1970**, *8*, 138–142.

(19) Jentoft, R. E.; Gouw, T. H. Apparatus for supercritical fluid chromatography with carbon dioxide as the mobile phase. *Anal. Chem.* **1972**, *44*, 681–686.

(20) Klesper, E.; Hartmann, W. Supercritical fluid chromatography of styrene oligomers. *J. Polym. Lett. Ed.* **1977**, *15*, 9–16.

(21) Hartmann, W.; Klesper, E. Preparative supercritical fluid chromatography of styrene oligomers. *J. Polym. Lett. Ed.* **1977**, *15*, 713–719.

(22) Novotny, M.; Springston, S. R.; Peaden, P. A.; Fjeldsted, J. C.; Lee, M. L. Capillary supercritical fluid chromatography. *Anal. Chem.* **1981**, *53*, 407–414.

(23) Gere, D. R.; Board, R.; McManigill, D. Supercritical fluid chromatography with small particle diameter packed columns. *Anal. Chem.* **1982**, *54*, 736–740.

(24) Witkowski, A.; Majkut, M.; Rulik, S. Analysis of pipeline transportation systems for carbon dioxide sequestration. *Arch. Thermodyn.* **2014**, *35*, 117–140.

(25) Tarafder, A.; Guiochon, G. Use of isopycnic plots in designing operations of supercritical fluid chromatography: I. The critical role of density in determining the characteristics of the mobile phase in supercritical fluid chromatography. *J. Chromatogr. A* **2011**, *1218*, 4569–4575.

(26) Tarafder, A.; Guiochon, G. Use of isopycnic plots in designing operations of supercritical fluid chromatography: II. The isopycnic plots and the selection of the operating pressure–temperature zone in supercritical fluid chromatography. *J. Chromatogr. A* **2011**, *1218*, 4576–4585.

(27) Tarafder, A.; Guiochon, G. Use of isopycnic plots in designing operations of supercritical fluid chromatography. III: Reason for the low column efficiency in the critical region. *J. Chromatogr. A* **2011**, *1218*, 7189–7195.

(28) Tarafder, A.; Kaczmarski, K.; Ranger, M.; Poe, D. P.; Guiochon, G. Use of the isopycnic plots in designing operations of supercritical fluid chromatography: IV. Pressure and density drops along columns. *J. Chromatogr. A*, *1238*, 132–145.

(29) Tarafder, A.; Kaczmarski, K.; Poe, D. P.; Guiochon, G. Use of the isopycnic plots in designing operations of supercritical fluid chromatography. V. Pressure and density drops using mixtures of carbon dioxide and methanol as the mobile phase. *J. Chromatogr. A* **2012**, *1258*, 136–151.

(30) Tarafder, A.; Guiochon, G. Unexpected retention behavior of supercritical fluid chromatography at the low density near critical region of carbon dioxide. *J. Chromatogr. A* **2012**, *1229*, 249–259.

(31) Novotny, M.; Bertsch, W.; Zlatkis, A. Temperature and pressure effects in supercritical-fluid chromatography. *J. Chromatogr. A* **1971**, *61*, 17–28.

(32) Berger, T.; Deye, J. Effect of mobile phase density gradients on efficiency in packed column supercritical fluid chromatography. *Chromatographia* **1990**, *30*, 57–60.

(33) Berger, T. The effect of adsorbed mobile phase components on the retention mechanism, efficiency, and peak distortion in supercritical fluid chromatography. *Chromatographia* **1993**, *37*, 645–652.

(34) Poe, D. P.; Schroden, J. J. Effects of pressure drop, particle size and thermal conditions on retention and efficiency in supercritical fluid chromatography. *J. Chromatogr. A* **2009**, *1216*, 7915–7926.

(35) Kaczmarski, K.; Poe, D. P.; Guiochon, G. Numerical modeling of elution peak profiles in supercritical fluid chromatography. Part I-Elution of an unretained tracer. *J. Chromatogr. A* **2010**, *1217*, 6578–6587.

(36) Lesellier, E.; West, C. The many faces of packed column supercritical fluid chromatography-A critical review. *J. Chromatogr. A* **2015**, *1382*, 2–46.

(37) Beckman, E. J. Supercritical and near-critical CO_2 in green chemical synthesis and processing. *J. Supercrit. Fluids* **2004**, *28*, 121–191.

(38) Wells, P. S.; Zhou, S.; Parcher, J. F. Unified chromatography with CO_2-based binary mobile phases. *Anal. Chem.* **2003**, *75*, 18–24.

(39) Tarafder, A. Metamorphosis of supercritical fluid chromatography to SFC: An overview. *TrAC Trends Anal. Chem.* **2016**, *81*, 3–10.

(40) Majors, R.; Berger, B.; Berger, T. A review of column developments for supercritical fluid chromatography. *LCGC North America* **2010**, *28*, 344–357.

(41) Cui, Y.; Olesik, S. V. Reversed-phase high-performance liquid chromatography using enhanced-fluidity mobile phases. *J. Chromatogr. A* **1995**, *691*, 151–162.

(42) Lee, S. T.; Olesik, S. V. Normal-phase high-performance liquid chromatography using enhanced-fluidity liquid mobile phases. *J. Chromatogr. A* **1995**, *707*, 217–224.

(43) Lee, S. T.; Reighard, T. S.; Olesik, S. V. Phase diagram studies of methanol-H_2O-CO_2 and acetonitrile-H_2O-CO_2 mixtures. *Fluid Ph. Equilib.* **1996**, *122*, 223–241.

(44) Olesik, S. V. Physicochemical properties of enhanced-fluidity liquid solvents. *J. Chromatogr. A* **2004**, *1037*, 405–410.

(45) Bennett, R.; Biba, M.; Liu, J., et al. Enhanced fluidity liquid chromatography: A guide to scaling up from analytical to preparative separations. *J. Chromatogr. A* **2019**, *1595*, 190–198.

(46) Van Konynenburg P. H.; L., S. R. Critical lines and phase equilibria in binary van der Waals mixtures. *Philos. Trans. R. Soc. A* **1980**, *298*, 495–540.

(47) Chester, T. L. The road to unified chromatography: The importance of phase behavior knowledge in supercritical fluid chromatography and related techniques, and a look at unification. *Microchem. J.* **1999**, *61*, 12–24.

(48) Gritti, F. Unexpected retention and efficiency behaviors in supercritical fluid chromatography: A thermodynamic interpretation. *J. Chromatogr. A* **2016**, *1468*, 209–216.

(49) Nilsson, L. B.; Westerlund, D. Peak compression effects in ion-pair reversed-phase liquid chromatography of substituted benzamides. *Anal. Chem.* **1985**, *57*, 1835–1840.

(50) Lesellier, E. Usual, unusual and unbelievable retention behavior in achiral supercritical fluid chromatography: Review and discussion. *J. Chromatogr. A* **2020**, *1614*, 460582.

(51) Enmark, M.; Åsberg, D.; Shalliker, A.; Samuelsson, J.; Fornstedt, T. A closer study of peak distortions in supercritical fluid chromatography as generated by the injection. *J. Chromatogr. A* **2015**, *1400*, 131–139.

(52) Guiochon, G.; Felinger, A.; Shirazi, D. G.; Katti, A. M., *Fundamentals of Preparative and Nonlinear Chromatography*, 2nd; Academic Press: Amsterdam, 2006.

(53) Felinger, A.; Zhou, D.; Guiochon, G. Determination of the single component and competitive adsorption isotherms of the 1-indanol enantiomers by the inverse method. *J. Chromatogr. A* **2003**, *1005*, 35–49.

(54) Felinger, A.; Cavazzini, A.; Guiochon, G. Numerical determination of the competitive isotherm of enantiomers. *J. Chromatogr. A* **2003**, *986*, 207–225.

(55) Enmark, M.; Forssén, P.; Samuelsson, J.; Fornstedt, T. Determination of adsorption isotherms in supercritical fluid chromatography. *J. Chromatogr. A* **2013**, *1312*, 124–133.

(56) Samuelsson, J.; Undin, T.; Törncrona, A.; Fornstedt, T. Improvement in the generation of adsorption isotherm data in the elution by characteristic points method-The ECP-slope approach. *J. Chromatogr. A* **2010**, *1217*, 7215–7221.

(57) Samuelsson, J.; Fornstedt, T. Injection technique for generating accurate adsorption isotherm data using the elution by characteristic points method. *Anal. Chem.* **2008**, *80*, 7887–7893.

(58) Cavazzini, A.; Felinger, A.; Guiochon, G. Comparison between adsorption isotherm determination techniques and overloaded band profiles on four batches of monolithic columns. *J. Chromatogr. A* **2003**, *1012*, 139–149.

(59) Vajda, P.; Guiochon, G. Determination of the column hold-up volume in supercritical fluid chromatography using nitrous-oxide. *J. Chromatogr. A* **2013**, *1309*, 96–100.

(60) Tarafder, A.; Guiochon, G. Accurate measurements of experimental parameters in supercritical fluid chromatography. I. Extent of variations of the mass and volumetric flow rates. *J. Chromatogr. A* **2013**, *1285*, 148–158.

(61) Tarafder, A.; Vajda, P.; Guiochon, G. Accurate on-line mass flow measurements in supercritical fluid chromatography. *J. Chromatogr. A* **2013**, *1320*, 130–137.

(62) Forss, E.; Haupt, D.; Stålberg, O., et al. Chemometric evaluation of the combined effect of temperature, pressure, and co-solvent fractions on the chiral separation of basic pharmaceuticals using actual vs set operational conditions. *J. Chromatogr. A* **2017**, *1499*, 165–173.

(63) Enmark, M.; Glenne, E.; Leśko, M., et al. Investigation of robustness for supercritical fluid chromatography separation of peptides: Isocratic vs gradient mode. *J. Chromatogr. A* **2018**, *1568*, 177–187.

(64) Glenne, E.; Samuelsson, J.; Leek, H., et al. Systematic investigations of peak distortions due to additives in supercritical fluid chromatography. *J. Chromatogr. A* **2020**, *1621*, 461048.

(65) Vajda, P.; Stankovich, J. J.; Guiochon, G. Determination of the average volumetric flow rate in supercritical fluid chromatography. *J. Chromatogr. A* **2014**, *1339*, 168–173.

(66) Poe, D. P.; Veit, D.; Ranger, M., et al. Pressure, temperature and density drops along supercritical fluid chromatography columns. I. Experimental results for neat carbon dioxide and columns packed with 3- and 5-micron particles. *J. Chromatogr. A* **2012**, *1250*, 105–114.

(67) Poe, D. P.; Veit, D.; Ranger, M., et al. Pressure, temperature and density drops along supercritical fluid chromatography columns in different thermal environments. III. Mixtures of carbon dioxide and methanol as the mobile phase. *J. Chromatogr. A* **2014**, *1323*, 143–156.

(68) Pauw, R. D.; Choikhet, K.; Desmet, G.; Broeckhoven, K. Temperature effects in supercritical fluid chromatography: A trade-off between viscous heating and decompression cooling. *J. Chromatogr. A* **2014**, *1365*, 212–218.

(69) Enmark, M.; Åsberg, D.; Leek, H., et al. Evaluation of scale-up from analytical to preparative supercritical fluid chromatography. *J. Chromatogr. A* **2015**, *1425*, 280–286.

(70) Enmark, M.; Samuelsson, J.; Fornstedt, T. A retention-matching strategy for method transfer in supercritical fluid chromatography: Introducing the isomolar plot approach. *Anal. Chem.* **2021**, *93*, 6385–6393.

(71) Glenne, E.; Leśko, M.; Samuelsson, J.; Fornstedt, T. Impact of methanol adsorption on the robustness of analytical supercritical fluid chromatography in transfer from SFC to UHPSFC. *Anal. Chem.* **2020**, *92*, 15429–15436.

(72) Gurdale, K.; Lesellier, E.; Tchapla, A. Study of dead volume measurement in packed subcritical fluid chromatography with ODS columns and carbon dioxide-modifier mobile phases. *J. Chromatogr. A* **2000**, *866*, 241–251.

(73) Vajda, P.; Guiochon, G. Modifier adsorption in supercritical fluid chromatography onto silica surface. *J. Chromatogr. A* **2013**, *1305*, 293–299.

(74) Vajda, P.; Guiochon, G. The modeling of overloaded elution band profiles in supercritical fluid chromatography. *J. Chromatogr. A* **2014**, *1333*, 116–123.

(75) Gritti, F.; Kazakevich, Y.; Guiochon, G. Measurement of hold-up volumes in reverse-phase liquid chromatography: Definition and comparison between static and dynamic methods. *J. Chromatogr. A* **2007**, *1161*, 157–169.

(76) Ismail, O. H.; Ciogli, A.; Villani, C., et al. Ultra-fast high-efficiency enantioseparations by means of a teicoplanin-based chiral stationary phase made on sub-2μm totally porous silica particles of narrow size distribution. *J. Chromatogr. A* **2016**, *1427*, 55–68.

(77) Åsberg, D.; Enmark, M.; Samuelsson, J.; Fornstedt, T. Evaluation of co-solvent fraction, pressure and temperature effects in analytical and preparative supercritical fluid chromatography. *J. Chromatogr. A* **2014**, *1374*, 254–260.

(78) Dascalu, A.-E.; Ghinet, A.; Billamboz, M.; Lipka, E. Performance comparison of chlorinated chiral stationary phases in supercritical fluid chromatography for separation of selected pyrrolidone derivatives. *J. Pharm. Anal.* **2019**, *9*, 248–253.

(79) Felinger, A., *Data Analysis and Signal Processing in Chromatography*, 1st Edition; Elsevier Science: Amsterdam, 1998.

(80) Ismail, O. H.; Pasti, L.; Ciogli, A., et al. Pirkle-type chiral stationary phase on core-shell and fully porous particles: Are superficially porous particles always the better choice toward ultrafast high-performance enantioseparations? *J. Chromatogr. A* **2016**, *1466*, 96–104.